PHILOSOPHICAL TRANSACTIONS OF THE ROYAL SOCIETY B BIOLOGICAL SCIENCES

Electron Microscopy of Molluscan Crossed-Lamellar Microstructure

N. V. Wilmot, D. J. Barber, J. D. Taylor and A. L. Graham

Phil. Trans. R. Soc. Lond. B 1992 **337**, 21-35
doi: 10.1098/rstb.1992.0080

Electron microscopy of molluscan crossed-lamellar microstructure

N. V. WILMOT[1], D. J. BARBER[2], J. D. TAYLOR[1]† AND A. L. GRAHAM[3]

[1] *Department of Zoology, The Natural History Museum, London SW7 5BD, U.K.*
[2] *Department of Physics, University of Essex, Colchester CO4 3SQ, U.K.*
[3] *Department of Mineralogy, The Natural History Museum, London SW7 5BD, U.K.*

SUMMARY

The morphology of the molluscan shell microstructure cross-lamellar structure (XLM) was studied by a scanning electron microscopy (SEM) examination of a variety of species (*Patella vulgata*, *Littorina littorea*, *L. nigrolineata*, *L. obtusata*, *L. saxatilis*, *Oliva sayana*, *Conus litteratus*, *C. magus*, *Pomatias elegans*, *Acanthopleura brevispinosa*, and *Arca tetragona*). Two of the gastropod species (*O. sayana* and *L. littorea*) were also examined by transmission electron microscopy (TEM) to determine the crystallographic relationships between the microstructural units.

SEM studies reveal that although the basic structure of XLM is broadly similar in all species, there is quite a degree of variation present in size of unit and regularity in form, even within a single specimen. Transitions from other aragonitic microstructures to XLM are gradational in nature, whereas the boundary between XLM and a calcitic microstructure is always sharp.

The basic morphological units in *Oliva sayana* are third order lamellae that are bounded by (001) and (1$\bar{1}$0) faces. They are profusely twinned on (1$\bar{1}$0) and have very minor (110) twinning. The crystallographic relationship between first order lamellae in *O. sayana* maintains an approximate parallelism between the (1$\bar{1}$0) twinning planes in adjacent crossed bands, and the third order lamellae in the bands are rotated by approximately 45° with respect to each other about the [001] direction.

The basic morphological units in *Littorina littorea* are third order lamellae with (001) and (100) faces, again with ubiquitous (1$\bar{1}$0) twinning. The crystallographic relationship between first order lamellae is an approximately 50° rotation about [100], making the [001] direction in the (100) face on a third order lamella of one band almost parallel to the [011] direction in the (100) face of a lamella of an adjacent band.

The organic interlamellar sheets are thought to control the inexact epitaxial relationships observed in both species, and our results indicate the likelihood of a unique matrix composition for each.

1. INTRODUCTION

Microstructures of molluscan shells are well known and can be classified into six main types: prismatic, nacreous, crossed lamellar, foliated, homogeneous, and spherulitic (see reviews by Wilbur & Saleuddin (1983); Watabe (1984); Carter & Clark (1985); and Carter (1990)). Initial descriptions were based on light microscope studies (Bøggild 1930; MacClintock 1967) with further advances generated by electron microscopy (Kobayashi 1964, 1971; Taylor *et al.* 1969, 1973; Grégoire 1972). Although the predominant shell mineralogies have been found to be aragonite and calcite, the detailed crystallography of the calcium carbonate crystals has rarely been determined. More emphasis has been placed on the composition, structure and function of the organic matrix that occurs in intimate association with the biominerals.

Crossed-lamellar structure (XLM) is by far the most common shell microstructure found in molluscs, occurring in the classes Bivalvia, Gastropoda, Scaphopoda and Polyplacophora. Indeed, most gastropod shells are formed of two to four layers of XLM aligned in different orientations. Despite its importance as a constructional material, and in contrast to the many investigations of nacreous and prismatic structure, the morphology of XLM is relatively poorly known, especially in the early stages of development. Previous work on XLM (Kobayashi 1964, 1971; Taylor *et al.* 1969; Zischke *et al.* 1970; Wise 1971; Uozumi *et al.* 1972; Grégoire 1972; Laghi & Russo 1978; Bandel 1979, 1990; Nakahara *et al.* 1981), has documented the structure and dimensions of the microstructure from a variety of molluscs. Typically, the mineralogy is aragonite, although some patellogastropods (limpets) also secrete a calcitic variety termed 'crossed-foliated' (MacClintock 1967). The crystals are arranged into bands (first order lamellae) lying parallel or radial to the shell margin (figure 1). These are composed of smaller units, often sheet-like in morphology (second order lamellae), which dip relative to the shell margin. Second order lamellae in adjacent first order lamellae dip in opposite directions, and the

† To whom correspondance should be sent.

Phil. Trans. R. Soc. Lond. B (1992) **337**, 21–35
Printed in Great Britain

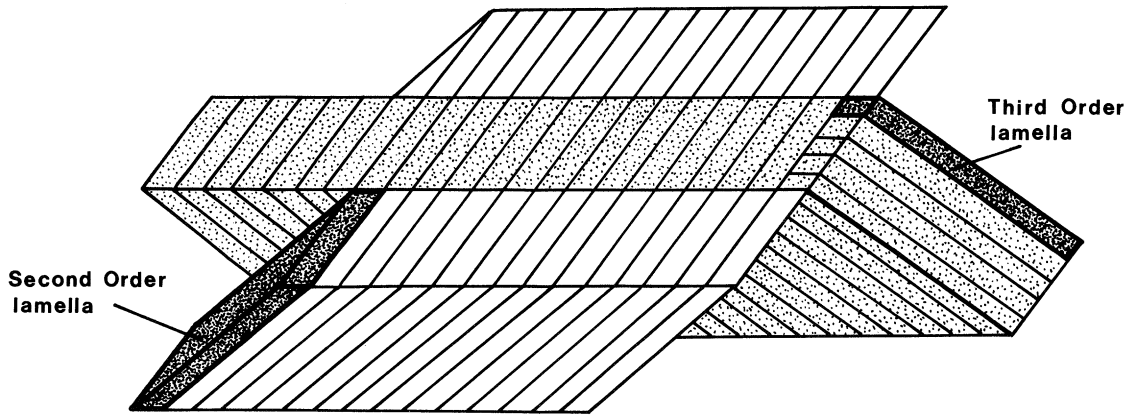

Figure 1. Simplified diagram of crossed lamellar structure, showing three first order lamellae. Based on Bøggild (1930, fig. 2) and MacClintock (1967, Text-fig. 19).

angles between them are typically 90–130° (Bandel 1979). Second order lamellae are subdivided into rods of third order lamellae (figure 1 and 2) which are surrounded by a thin layer of organic material (Uozumi *et al.* 1972; Nakahara *et al.* 1981). The widths of first order lamellae vary from less than 10 μm to over 40 μm (Carter & Clark 1985), with third order lamellae 0.3–2.0 μm wide, and more than 10 μm long (Wise 1971; Uozumi *et al.* 1972). Crossed-lamellar structure exhibits many minor variations in different mulluscan groups and these are described by Carter and Clark (1985).

The aims of this study are to investigate the morphology and development of aragonitic XLM, and determine the crystallographic orientation of the crystals in the different morphological units using electron diffraction patterns. Although the precise crystallographic orientation of some molluscan microstructures has been found through electron diffraction, such as for nacre (Weiner *et al.* 1983) and foliated calcite (Runnegar 1984), the only published data concerning aragonitic XLM are based on light microscope observations (Bøggild 1930; Haas 1972), and TEM studies of third order lamellae from a marine gastroped (Laraia & Heuer 1990; Laraia *et al.* 1990). An increased knowledge of XLM morphology, especially in its initial stages of development may lead to a better understanding of the process of shell secretion.

2. MATERIAL AND METHODS

Shell material from the following species were examined by scanning electron microscopy (SEM); gastropods *Patella vulgata* Linnaeus, *Littorina littorea* (Linnaeus), *L. nigrolineata* Gray, *L. obtusata* (Linnaeus), *L. saxatilis* (Olivi), *Oliva sayana* Ravenel, *Conus litteratus* Linnaeus, *C. magus* Linnaeus, *Pomatias elegans* (Müller), chiton *Acanthopleura brevispinosa* (Sowerby), bivalve *Arca tetragona* Poli.

Oliva sayana and *Littorina littorea* were also examined by transmission electron microscopy (TEM).

All material is housed in the Mollusca Division, Department of Zoology, The Natural History Museum, London.

(*a*) *SEM*

For surface views, shells were trimmed with a microsaw ready for mounting on 13 mm aluminium pin stubs. For orientated sections, shells were first embedded in epoxy resin (Araldite) to prevent loss of outer layers during sectioning. The slices were then polished and washed in an ultrasonic bath, etched in hydrochloric acid (10% by volume) and washed in distilled water before mounting on 13 mm aluminium pin stubs with Araldite. Samples were air dried and coated with gold-palladium, with a Polaron E5000 sputter coater, before examination with a Hitachi S-800 scanning electron microscope.

(*b*) *TEM*

Orientated thin-sections, mounted with a thermoplastic acetone-soluble adhesive (Crystalbond 509), were made from shells previously embedded in Araldite. Copper rings (1500 μm) were then glued onto

Figure 2. Scanning electron micrographs of crossed lamellar structure. (*a*) *Oliva sayana*. Etched transverse section through first order lamellae. Irregular fractures are probably generated during polishing of the specimen. Scale bar = 10 μm. (*b*) *Arca tetragona*. Partly broken growth surface with prominant first order lamellae. The different orientations of the third order lamellae are clearly seen on the fracture plane (top right). Scale bar = 20 μm. (*c*) *Conus litteratus*. Two first order lamellae seen on a growth surface, with numerous second order lamellae running left to right. Scale bar = 1 μm. (*d*) *Patella vulgata*. Growth surface showing the boundary of two aragonitic XLM first order lamellae subdivided into third order lamellae of unequal widths. Note how the second order lamellae are stacked 'en echelon', and that their widths do not correspond to the true breadth of the third order lamellae. Scale bar = 1 μm. (*e*) *Arca tetragona*. Growth surface showing boundary between two first order lamellae. Note the numerous third order lamellae, but no formal arrangement into second order lamellae (as in *b* and *c*). Scale bar = 1 μm. (*f*) *Oliva sayana*. Acicular third order lamellae seen on a fracture surface. Scale bar = 1 μm.

PHILOSOPHICAL TRANSACTIONS OF THE ROYAL SOCIETY B BIOLOGICAL SCIENCES

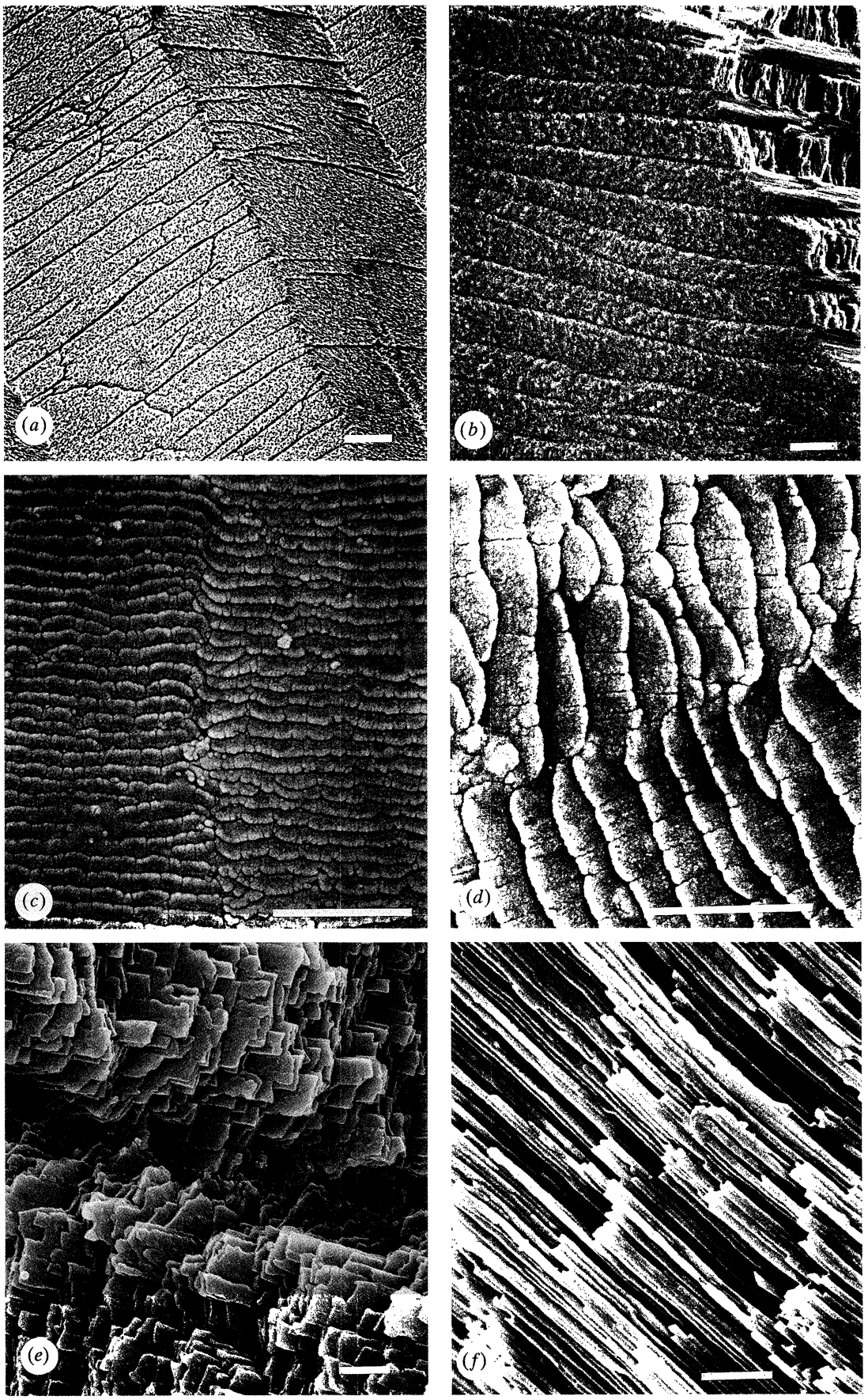

Figure 2.

PHILOSOPHICAL TRANSACTIONS OF THE ROYAL SOCIETY B BIOLOGICAL SCIENCES

Table 1.

species	first order lamella micrometres	second order lamella (growth surf.) micrometres	third order lamella micrometres width	third order lamella micrometres breadth	angle degrees
Patella vulgata	2–8	0.25	0.1–0.4	0.05	55
Littorina spp.	2–8.5	N/A	0.2–0.4	0.09	50–90
Oliva sayana	10–30	N/A	0.05–0.28	0.03–0.05	45–70
Conus litteratus	13	0.1	0.04–0.25	0.03–0.08	78–90
Conus magus	10–25	N/A	0.1–0.2	0.07–0.08	56–85
Pomatias elegans	7.5–12.5	N/A	0.08–0.28	0.04–0.08	40–87
Acanthopleura brevispinosa	1.7–5	N/A	—	0.1–0.6	32–45
Arca tetragona	7.5–28	N/A	0.08–0.6	0.03–0.15	32–45

the sections with Araldite and allowed to set. The sections were later soaked off their glass mounts with acetone and allowed to dry. Further copper rings were then mounted onto the reverse side of the sections, immediately behind the original ones. Once set, the rings were cut away from the excess material and ion-thinned with an Iontech Super Microlap Mark 2 B306 ion-thinner and lightly carbon-coated.

Other workers have commented on the susceptibility of biogenic aragonite (cf. inorganic aragonite) to ion irradiation (e.g. Laraia *et al.* 1990) and high intensity electron irradiation (Ness *et al.* 1990; Laraia *et al.* 1990). Biogenic aragonite is less stable against particle irradiations than inorganic (Burrage & Pitkethly 1969; McTigue & Wenk 1985). The two forms may also degrade to different end-products although this is probably a function of the state of disaggregation (Laraia *et al.* 1990). Ion-induced and electron irradiation damage of aragonite is most serious when undertaking high resolution imaging. We did not find either to be a serious problem with the species that we investigated using conventional TEM methods, and there was no need to resort to minimal exposure techniques (see Williams & Fisher 1970). We did not attempt any high resolution lattice imaging, which would have required higher electron beam intensities. Our TEM studies were all carried out using a JEOL 200-CX microscope, equipped with a double tilt stage, and operated at 200 kV, with a nominal camera length in diffraction of 137 cm.

In addition to making integral TEM ion-thinned sections from the shells, disaggregated crystals were obtained and examined to establish the nature of the basic morphological units constituting XLM. This was achieved by scraping a chosen area of the inner surface of a shell with a scalpel blade, collecting the resulting loose material in a 5 ml beaker, adding a few drops of alcohol and applying ultrasonic vibration. An electron microscope grid supporting a carbon film was then dragged through the liquid to collect some of the carbonate fragments. The grid was then allowed to dry before a thin coating of carbon was evaporated onto the fragment-laden film surface in order to secure and stabilize the carbonate material.

3. RESULTS

We regret the confusing terminology regarding the various levels (or 'orders') of structural unit present in XLM. A 'second order lamella' refers to a particular arrangement of 'third order lamellae' which is often not present. However, as the terms are now well established in molluscan literature we felt it inappropriate to change them now.

4. SEM RESULTS

Dimensions of XLM obtained by this study are summarised in table 1. One of the main points to emerge is that the various components forming XLM are actually quite variable in size, even in a single specimen. Although diagrams such as figure 1 are useful in conveying the broad features of the structure, they imply a much greater regularity in form than is actually present. The boundaries between first order lamellae, and their overall shapes are irregular (figure 2*b*, *d*), as are the widths of third order lamellae (figures 2*e* and 3). Some third order lamellae are needle-like in form (figure 2*f*), and not all species have third order lamellae arranged into 'sheets' of second order lamellae (figure 2*e*, *f*).

As previously reported by Bandel (1979), the angle of inclination between third order lamellae in adjacent first order lamellae varies within an individual mollusc and cannot be used as a taxonomic aid. Such angles are difficult to measure precisely from sections as the orientation through the specimen affects the apparent dip. Moreover, because of the presence of interleaved organic material and the possible integrated effects of strain and crystal defects, the existence of an exact crystallographic relationship adjacent lamellae is not precluded. We have been concerned to investigate this possibility by using TEM methods. Reported widths of second order lamellae must also be treated with caution as dimensions obtained from growth surfaces may not represent the true widths if the lamellae are stacked 'en echelon' (figures 2*d*, and 3).

Third order lamellae may have pitted surfaces (figure 3); a feature not previously commented upon, although illustrated by Carter & Lutz (1990, plate 79, figure 8). Such pitting was seen in *Patella vulgata*, *Conus litteratus*, *Pomatias elegans* and *Arca tetragona*, and was only exposed on fracture surfaces, never on growth surfaces (figure 3). As the pits have not been observed using TEM they may be artefacts generated during fracture.

Although some growth surfaces are covered by an organic membrane, the amount of organic matter

PHILOSOPHICAL TRANSACTIONS OF THE ROYAL SOCIETY B BIOLOGICAL SCIENCES

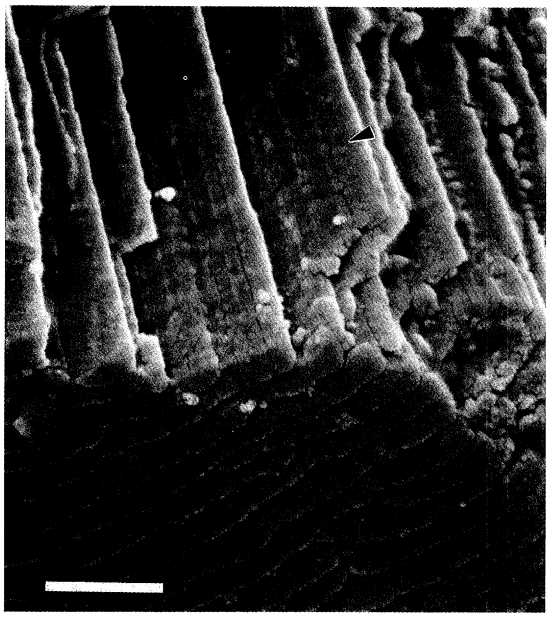

Figure 3. Pits on third order lamellae, exposed on fracture surfaces of *Patella vulgata*. Note the difference between the actual width of third order lamellae as seen on the fracture surface, compared with their apparent width on the growth surface. Scale bar = 1 μm.

present in XLM is very small. Nakahara *et al.* (1981) noted the presence of thin organic envelopes surrounding third order lamellae, and we have not found any evidence of additional layers delimiting second or first order lamellae.

So far, 'mature' XLM has been described, however the initial stages seen at the margins of the shell growth surface are often less well ordered (figure 4). The extreme edge may consist of extremely fine, granular crystals, which gradually become elongated and orientated to form the regular XLM structure. XLM is secreted in one of three ways: (i) directly onto the periostracum; (ii) onto another layer of XLM, and (iii) onto a layer of different microstructure or mineralogy. When XLM is secreted onto the periostracum, the initial layer of crystals may be of different morphology to mature XLM (figure 5). Such initial layers are typically very thin (0.4–1.0 μm) and are composed of acicular crystals lying perpendicular to the shell surface (figure 5*a*). Alternatively, the thin primary layer may be composed of third order lamellae inclined in opposing directions, but not organised into first order lamellae (figure 5*b*). In all cases, the transition to XLM is gradational.

When XLM is laid down on another layer of XLM, the orientation of the first order lamellae is rotated by approximately 90°, which confers greater mechanical strength (Currey & Kohn 1976). The junction between the two layers is not abrupt, but characterized by 'feathering' of the first order lamellae (figure 6).

Some species have XLM preceded by aragonitic spherulitic layers, *Neptunea antiqua* has relatively thick spherulitic layers which develop on top of an eroded calcite surface. Once the surface has levelled again, XLM is generated (figure 7*a*). In *Pomatias elegans* the primary shell layer is a spherulitic-prismatic structure which then develops into XLM. The boundary between the microstructures may be gradational (figure 5*c*), or marked by a layer of acicular crystals perpendicular to the shell surface (figure 7*b–d*). The presence of an acicular layer is uncommon however, and may only occur sporadically within a specimen. Similar spherulitic–XLM associations have been described for *Laevilitorina bennetti* and *Bembicium auratum* (Taylor & Reid 1990, figures 21, 22).

The above observations demonstrate that transitions from aragonitic microstructures to XLM are

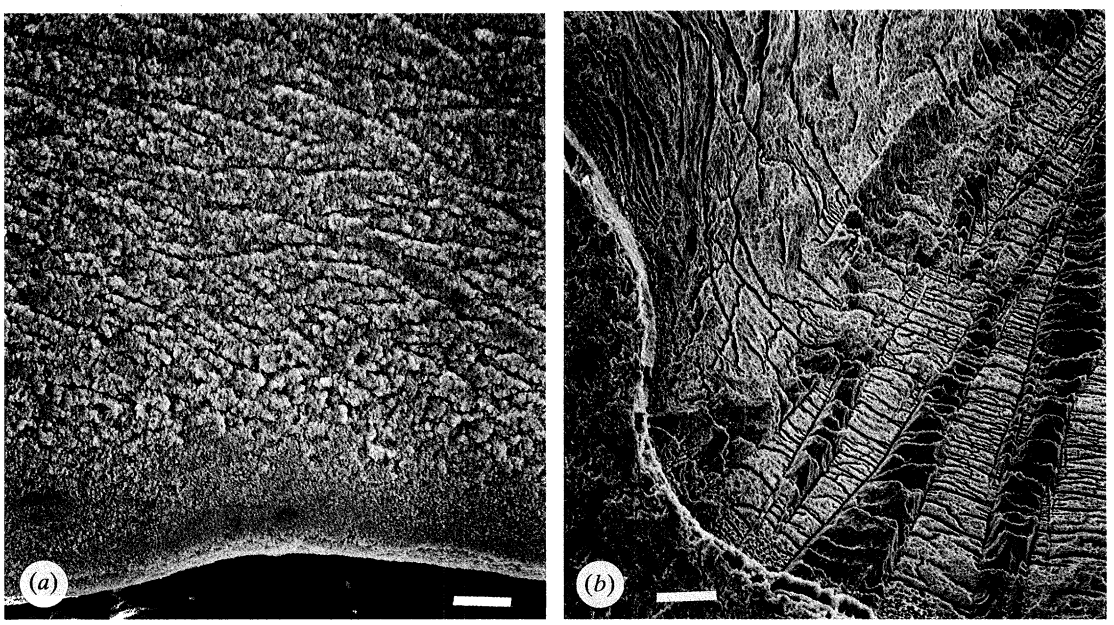

Figure 4. Margins of the shell growth surface of *Arca tetragona*. (*a*) Surface view showing a progression from fine homogeneous structure to more ordered first order lamellae. Eventually, regular first order lamellae are generated, as in figure 2*b*. Scale bar = 20 μm. (*b*) Etched radial section through the growth surface, with disorganized crystals grading into XLM. Scale bar = 20 μm.

PHILOSOPHICAL TRANSACTIONS OF THE ROYAL SOCIETY B BIOLOGICAL SCIENCES

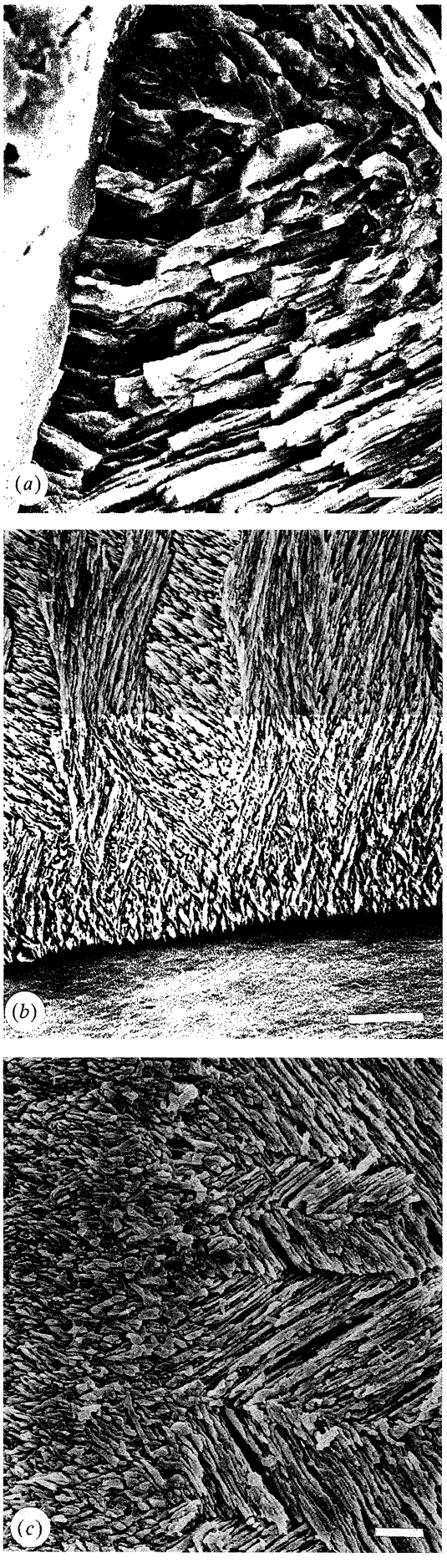

Figure 5 (*a*) *Oliva sayana*. Transverse section showing initial crystals lying perpendicular to the shell surface. Scale bar = 1 μm. (*b*) *Conus magus*. Etched radial section through the shell. Third order lamellae secreted directly onto the periostracum (bottom) are not initially organized into first order lamellae. Scale bar = 5 μm. (*c*) *Pomatias elegans*. Etched radial section showing gradual transition to XLM. Scale bar = 2 μm.

Figure 6. Etched radial section of *Conus magus* showing the boundary between two XLM layers. Scale bar = 20 μm.

gradational in nature. This has also been reported by other workers (Bandel 1979, 1990; Shimamoto 1986). In contrast, when XLM is laid down directly on a calcitic microstructure, the junction is always sharp, and often irregular (figure 8). Such abrupt transitions of mineralogy may also be marked by a concentration of organic matter (figure 8*a*) although this may not occur uniformly.

5. TEM RESULTS FROM *OLIVA SAYANA*

(*a*) *Basic morphological unit*

We selected for investigation those shell fragments which appeared to be individual crystals and to have fairly well-defined faces with a major face lying on the carbon film. TEM bright field images and the corresponding electron diffraction patterns were recorded for each crystal. These pairs of negatives were subsequently analysed (i) to check that each crystal was aragonite, and (ii) to determine how the morphology of each crystal related to the axes of the aragonite unit cell. In this way, one expected to establish crystal habit, i.e. either the indices of atomic planes which might constitute the crystal faces or possibly the indices of crystallographic directions lying parallel to the crystal axes. Some of the pairs of negatives gave ambiguous non-rational indices for the crystal face

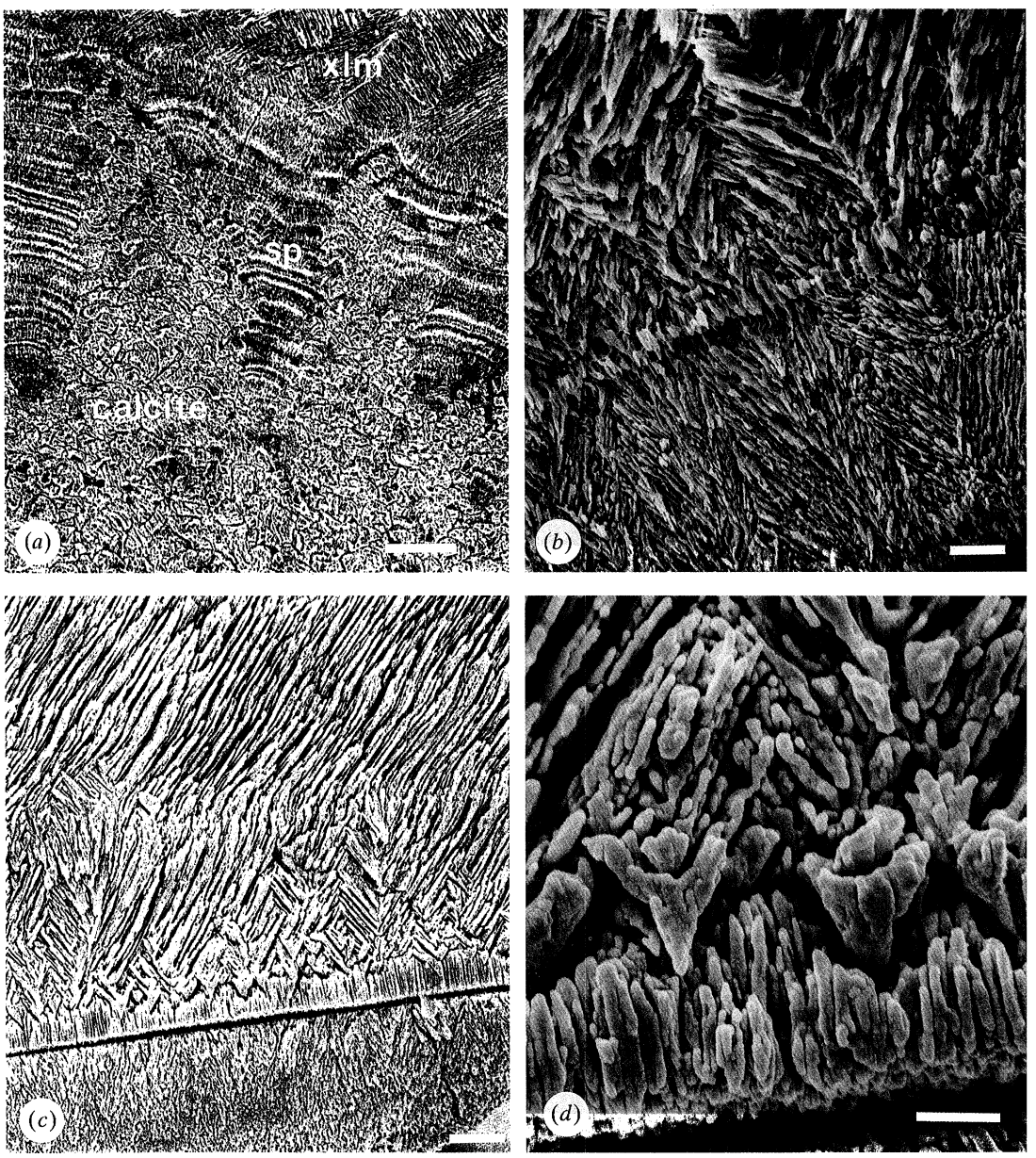

Figure 7. XLM preceded by a spherulitic layer. (*a*) *Neptunea antiqua*. Irregular cavities in blocky calcite (bottom) are filled by spherulitic structure (sp), which grades into XLM (top). Scale bar = 20 μm. (*b–d*) *Pomatias elegans*. Spherulitic-prismatic layer (bottom), overlain by XLM. (*b*) Etched radial section. Scale bar = 2 μm. (*c*) Well-defined layer of acicular crystals at the spherulite–XLM boundary marked by a line in the lower half of the photograph. Scale bar = 4 μm. (*d*) Close up of acicular crystals in (*c*). Scale bar = 1 μm.

which was supposedly in contact with the carbon support film (and therefore roughly perpendicular to the electron beam with the stage set at zero tilts). Such results were presumably a consequence of protuberances on the crystal surface, or loose but adhering smaller fragments.

Most of our findings indicate that the basic crystal unit in *O. sayana* is the third order lamella, and is bounded by (001) and (1$\bar{1}$0) faces (thus having a rectangular cross-section), with the major dimension perpendicular to the cross-section and parallel to the [110] direction. End-on views of these lamellae (next section) show (001) invariably to be the major face, with the (1$\bar{1}$0) face narrower. These third order lamellae are profusely and rather homogeneously twinned on (1$\bar{1}$0). Figure 9 illustrates such a crystal (which other observations show is only a short fragment of a lamella, see next section) while the inset is the corresponding [001] zone axis host-plus-twin diffraction pattern, consistent with (1$\bar{1}$0) twinning. It should be noted here that (1$\bar{1}$0) and (110) twinning are not equivalent in their effects at twin–host interfaces in heavily twinned aragonite, since exclusive use of the former avoids coherency strains (Laraia *et al.* 1990).

(*b*) *Crossed-lamellar structure*

The crystallographic relationship between lamellae in *O. sayana* is relatively simple. The third order

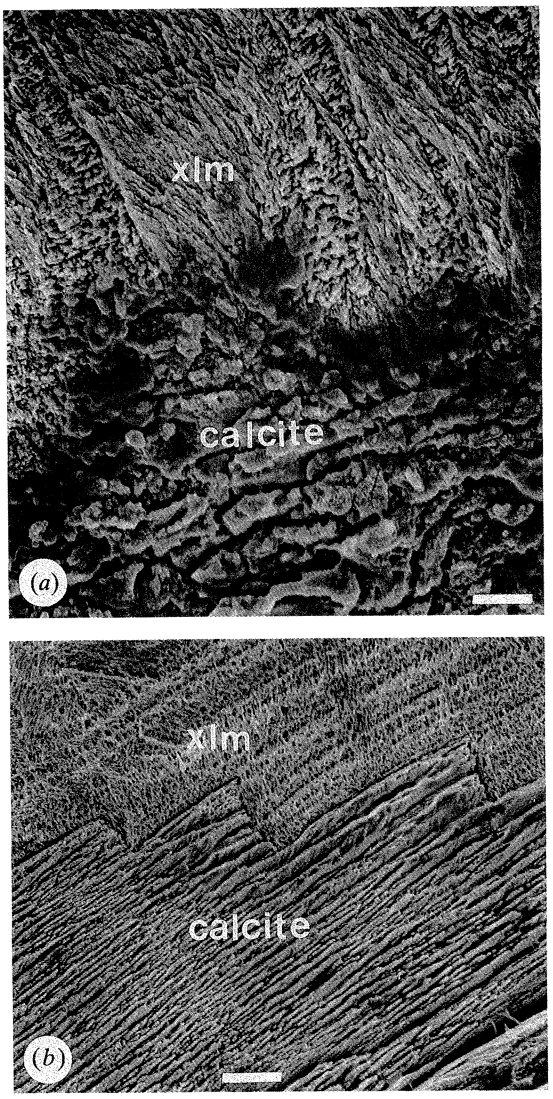

Figure 8. Abrupt, irregular junctions between calcite microstructures and XLM. (*a*) *Littorina littorea*. Note the concentration of darker organic matter at the boundary between blocky calcite (below) and XLM (above). Scale bar = 4 μm. (*b*) *Patella vulgata*. Aragonitic XLM above, calcitic crossed-foliated structure below. Scale bar = 10 μm.

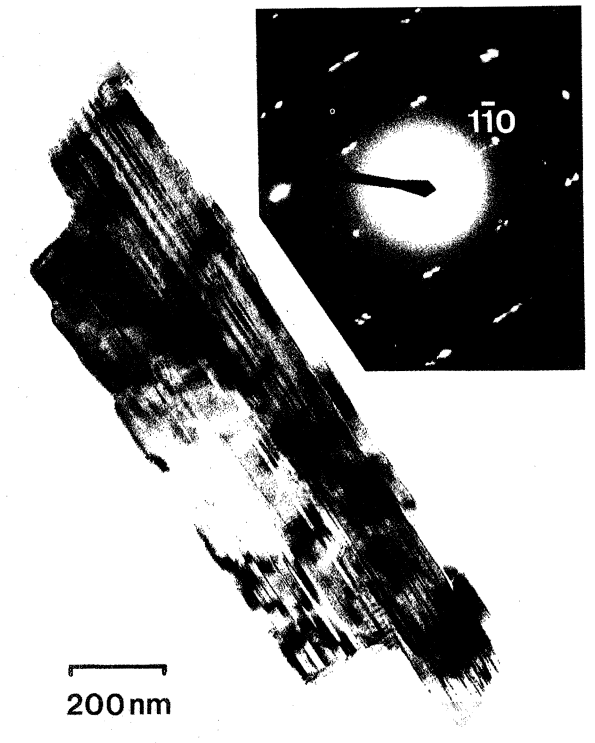

Figure 9. TEM image showing fragment of a single third order lamella from *Oliva sayana*, with multiple $(1\bar{1}0)$ twinning and corresponding [001] zone axis diffraction pattern (inset).

lamellae occur as bundles with a common axis [110] and the (001) major and $(1\bar{1}0)$ minor faces of adjacent lamellae respectively sub-parallel. The spread in orientations about [110] ranges up to about 30° over some hundred lamellae, and gives a strong texture to electron diffraction patterns obtained within a band, using a field aperture of diameter approximately 50 μm. The morphology of the lamellae is illustrated in figure 10*a*, *b*. Figure 10*a* is a fairly low magnification image which includes the boundary between two first order lamellae, and shows third order lamellae that are almost 'end-on' at top right, while they are 'sideways-on' at the lower left. The strong $[31\bar{2}]$ zone axis texture shown in figure 10*b* was obtained from 'end-on' lamellae.

The relationship between first order lamellae corresponds to the maintaining of an approximate parallelism between $(1\bar{1}0)$ planes in most third order lamellae, with a rotation across the first order boundary around the normal to the twin plane. The rotation varies somewhat from place to place, and there is a further uncertainty because the centre of symmetry of aragonite does not allow one to distinguish between the axes **c** and $-\mathbf{c}$ in conventional electron diffraction patterns. Figure 11*a*, *b* shows respectively, bright field and dark field images of a first order boundary region, the dark field image being recorded using the marked reflections seen in the inset diffraction pattern of figure 11*a* (field aperture centred on the boundary). The selected-area diffraction patterns (SADS) in figure 11*c*, *d* show respectively, the patterns from fields within the top half (A) of the micrograph and within the bottom half (B). The lengths of the lamellae in band A support the contention that the crystal shown in figure 9*a* was only a short length of lamella. The sub-parallel crystallographic alignment between lamellae in one first order lamella, set A, and of the $(1\bar{1}0)$ planes throughout both bands, A and B, is illustrated by the dark field image in figure 11*b*, recorded using part of arced $112_A/102_B$ reflections, which almost coincide (shown in the inset of figure 11*a*). A proportion of the lamellae appear bright, these being the ones that have their (110) planes parallel to within about 3°. Data from stereographic analysis of diffraction patterns show that the angle between the **c**-axes is approximately $30° \pm 15°$, an ambiguity that cannot be resolved solely on the basis of conventional electron diffraction, with a variability of several degrees on both possibilities. We favour the sum, i.e. 45°, because the greater degree of lamellar misorientation will be associated

PHILOSOPHICAL TRANSACTIONS OF THE ROYAL SOCIETY B BIOLOGICAL SCIENCES

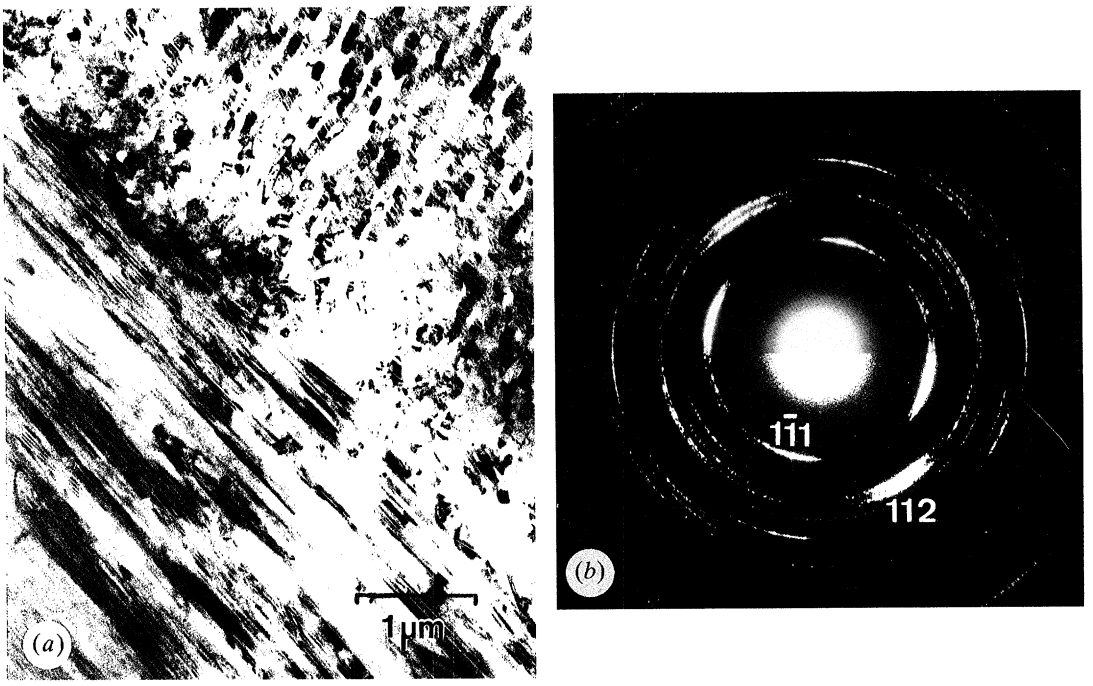

Figure 10. *Oliva sayana*. (*a*) TEM image of the boundary zone between first order lamellae, with one set of third order lamellae approximately 'end-on' and the other 'side-on'. Note the approximate parallelism of (1$\bar{1}$0) twinning across the boundary zone, although a few third order lamellae right at the boundary are strongly misorientated. (*b*) [31$\bar{2}$] zone axis diffraction pattern from 'end-on' third order lamellae in (*a*), showing strong texture.

with not only greater strength but with less strength anisotropy within the shell. It is clear that there is no exact epitactic relationship between third order lamellae belonging to the two sets of first order lamellae, but rather some form of biogenic switching of the orientation of the growth planes.

Those unpractised in interpreting TEM micrographs and diffraction patterns may have difficulty in understanding the information contained in the figures. Figure 12 is a sketch to illustrate what we believe to be the spatial relationship between two idealized third order lamellae across a first order boundary in *O. sayana*.

6. TEM RESULTS FROM *LITTORINA LITTOREA*

(*a*) *Basic morphological unit*

A similar procedure was used for investigating the crystallography of *L. littorea* third order lamellae. The results in this case are somewhat different. The major face on crystal fragments with well-defined geometric outlines is invariably (001), as with *O. sayana*. However, identifying a second major face for the *L. littorea* morphological unit was less successful. With most of our samples, the second principal face is (100), so that the major length is parallel to the [010] direction. An example is illustrated in figure 13*a*, together with the corresponding [001] zone axis diffraction pattern (inset). There was, however, puzzling evidence that this combination might not be unique and a few crystals appeared to have (001) and (110) faces. Where these fit into the interlamellar relationship found for *L. littorea* (next section) is not clear.

Twinning on (1$\bar{1}$0) is again very profuse, as in *O. sayana*. More rarely small regions are found within the third order lamellae of *L. littorea*, where very thin twins also occur on (110) (as with the crystal shown in figure 13*a*, although it is scarcely apparent). Within some of the broader (110) twin lamellae, there is sometimes further (1$\bar{1}$0) twinning. Figure 13*b*, again with inset SAD, illustrates another *L. littorea* crystal in which the presence of both twin laws is more obvious.

(*b*) *Crossed-lamellar structure*

The orientation relationships between the lamellae for *L. littorea* are less straightforward than for *O. sayana*. For example, it was immediately obvious from TEM images that the twins in the different sets of first order lamellae were not aligned. Figure 14*a* shows a typical view in which the ends of the third order lamellae interleave in a chevron arrangement. The terminations do not all completely abut, and so voids occur along the first order boundary. This may well indicate that the lamellae can grow edgewise, the organic membranes providing the necessary freedom for the relaxation of stresses resulting from the contact of any rough lamellar surfaces, as well as acting as a template (see discussion) for initial growth. Electron diffraction patterns, where taken from fields large enough to encompass many third order lamellae belonging to one set of first order, showed a strong complex texture. The misorientation between adjacent third order lamellae was investigated by electron

PHILOSOPHICAL TRANSACTIONS OF THE ROYAL SOCIETY B BIOLOGICAL SCIENCES

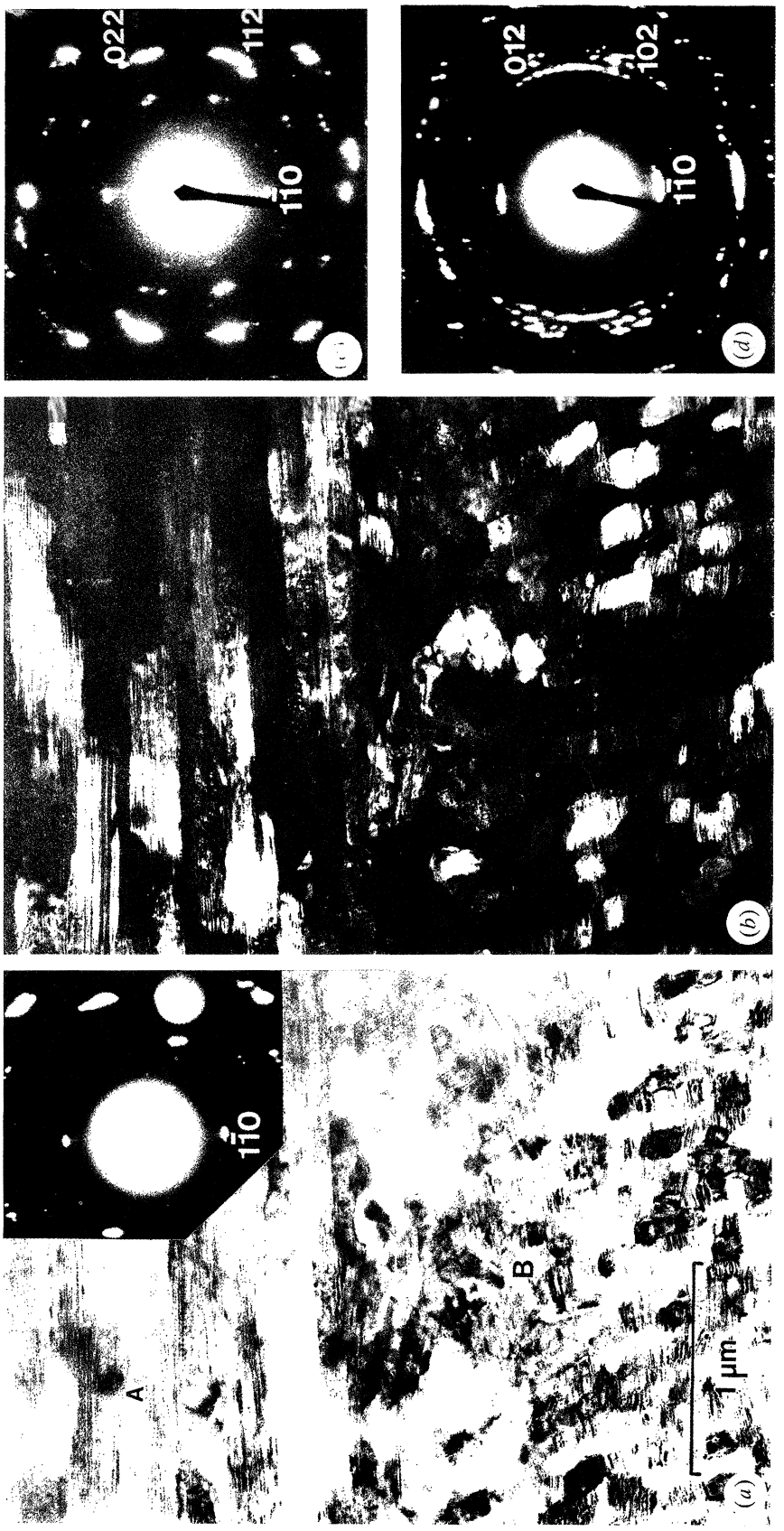

Figure 11. *Oliva sayana*. (*a*) Bright field TEM image of first order boundary zone and (inset) superposed selected area diffraction pattern (SAD) from the zone. Note (110) twinning and some porosity. (*b*) Centred dark field TEM image corresponding to (*a*), recorded with the objective aperture positioned around the almost coincident 112 and 102 reflections (from third order lamellae), as indicated in the inset of (*a*). (*c*) $[11\bar{1}]$ zone axis SAD, with minor arcing of reflections, from field near (A) in (*a*). (*d*) $[22\bar{1}]$ zone axis SAD, with strong arcing of relections, from field centred on (B) in (*a*).

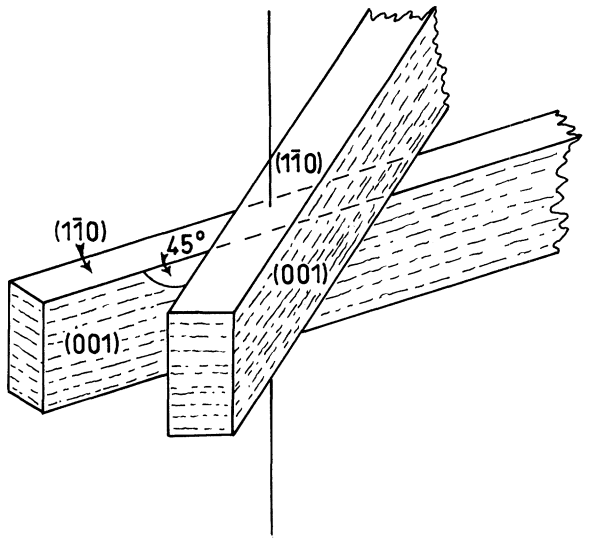

Figure 12. Sketch to illustrate the orientation relationship between two characteristic third order lamellae across a first order boundary in *Oliva sayana*. The relative rotation of the two lamellae is around the vertical axis, which is perpendicular to (1$\bar{1}$0). Dashed line region represents the orientation of the twin layers. The surfaces of the lamellae are shown as smooth planes for the sake of simplicity, not because there is any firm evidence for their being flat.

diffraction and gave interesting results. Reducing the size of the field aperture to encompass just a few lamellae invariably gave a diffraction pattern consistent with sub-parallel alignment of (001) planes. Such SADs are effectively the superposition of several slightly rotated [100] zone axis patterns, each corresponding to a single lamella and misorientated by a rotation of about 2° about the **a**-axis with respect to the patterns from the two directly adjacent lamella. The presence of even smaller misorientations between parts of some third order lamellae is clearly indicated by moiré fringes in many of the images from *L. littorea*, e.g. where arrowed in figure 14*a*.

Diffraction patterns from just a few interleaved third order lamellae, at the boundary zone of two first order lamellae were most revealing, since they showed a variable but reproducible crystallographic relationship between the first order bands of lamellae. The inset SAD of figure 14*a*, from an area of some 10 μm^2 at the boundary zone, arises from the superposition of two [100] zone axis patterns, figure 14*b*, *c* from the upper (A) and lower (B) sides of the zone respectively, which have a relative rotation of approximately 50°. This is indicated by figure 15*a*, which explains diagrammatically the combined diffraction patterns in the inset of figure 14*a*. The common **a**-axis suggests that in *L. littorea* it is the (100) faces of the basic crystal units (third order lamellae) that maintain the more precise parallelism, not (1$\bar{1}$0) as in *O. sayana*. Figure 14*b*, *c* implies that other crystallographic relationships hold at the abutting and overlapping ends of the third order lamellae: we find that $[001]_A$ is parallel to $[011]_B$ to within 4° and that the (031) planes of the A first order lamella are located parallel to the (03$\bar{1}$) planes in first order lamella B. Figure 15*b* is a sketch, based on the combined diffraction information, to illustrate what we have found as the relationship between two idealized third order lamellae across a first order boundary.

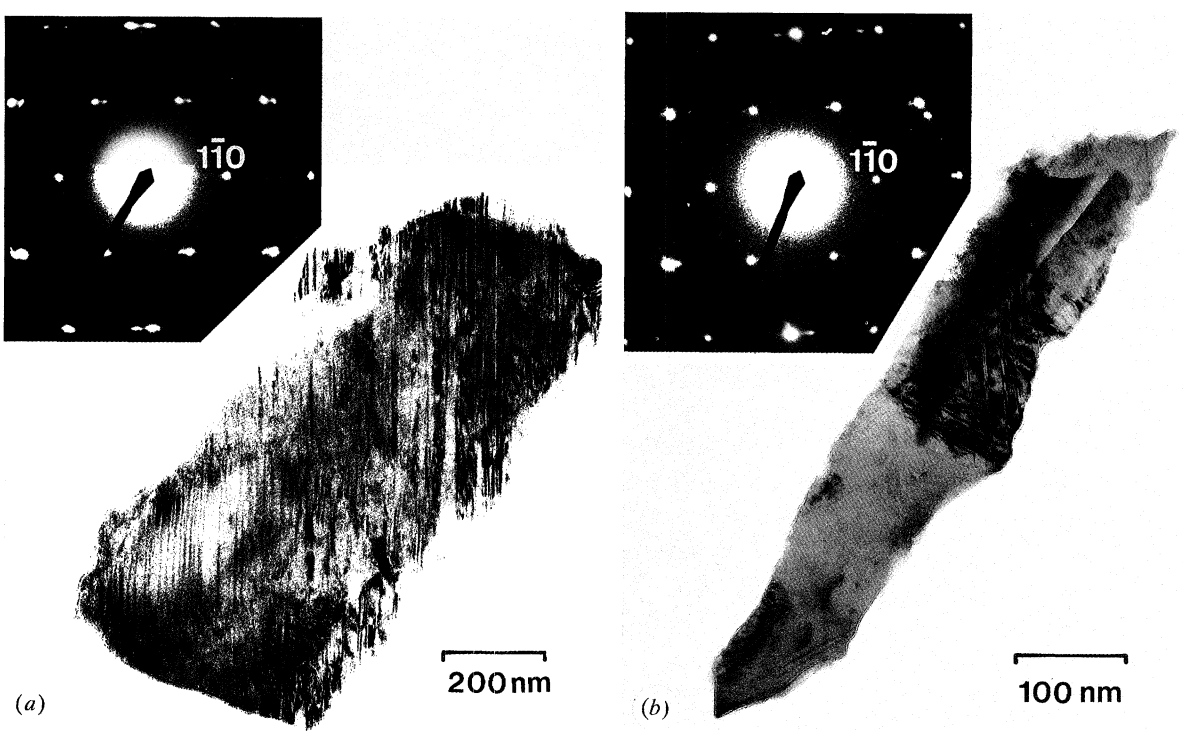

Figure 13. (*a*) TEM image of fragment of a single third order lamella from *Littorina littorea*, with multiple (1$\bar{1}$0) twinning and corresponding [001] zone axis diffraction pattern (inset). (*b*) TEM image of another fragment of a single third order lamella from *L. littorea*, showing both (1$\bar{1}$0) and (110) twinning, and with corresponding [001] zone axis diffraction pattern (inset).

PHILOSOPHICAL TRANSACTIONS OF THE ROYAL SOCIETY B BIOLOGICAL SCIENCES

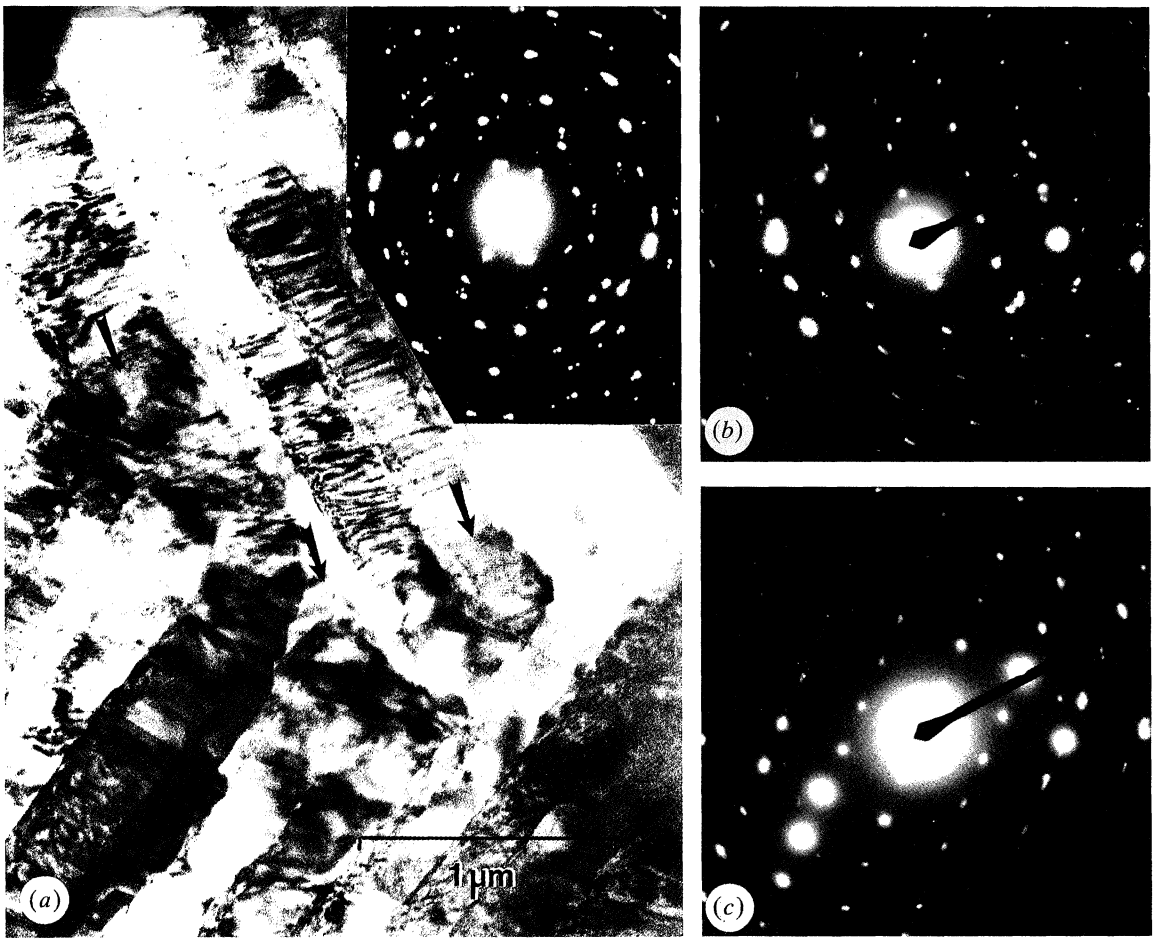

Figure 14. (*a*) TEM image of the boundary zone between first order lamellae in *Littorina littorea*, indicating interlocking of the ends of the third order lamellae. Arrows point to moiré patterns formed where overlapping parts of the lamellae are slightly misorientated. The SAD (inset) consists of two superposed [100] zone axis patterns. (*b*) [100] zone axis SAD obtained from lower part (A) of (*a*). (*c*) [100] zone axis SAD obtained from lower part (B) of (*a*).

Both species sometimes exhibited limited signs of beam damage in the form of fine porosity, especially at the margins of third order lamllae. This is similar to the 'frothy' texture in nacre discussed by Towe & Thompson (1972). Adjacent first order lamellae typically had markedly different levels of porosity, suggesting that damage is related to the angle of the electron beam with respect to the crystal faces.

7. DISCUSSION

Electron microscope studies have confirmed the basic structural units of mature XLM to be rectangular third order lamellae. The surprising results of this study reveal that although third order lamellae of different species have similar morphologies under SEM. they are in fact crystallographically distinct. We found the existence of a common sub-parallel $(1\bar{1}0)$ crystal plane in the *Oliva sayana* microstructure, and a common parallel (100) plane in *Littorina littorea*. The only previous crystallographic studies of XLM from the marine gastropod *Strombus gigas* (Laraia & Heuer 1990; Laraia *et al.* 1990) reported yet another common axis [112]. As found for *Strombus gigas* (Laraia *et al.* 1990), the aragonite crystals are subdivided into profuse microtwins almost exclusively on the $(1\bar{1}0)$ plane, which could be regarded as fourth order lamellae. The significance of the twinning is still unclear as it does not appear to be important to the crystallographic relationship between first order lamellae. The twin planes are approximately aligned across the first order bands in *O. sayana*, whereas they are at large angles in *L. littorea*. However, as noted by Laraia *et al.* (1990), and mentioned earlier, the almost total absence of (110) twinning (as commonly occurs together with $(1\bar{1}0)$ twinning in geological aragonites) minimizes coherency strains at twin–host interfaces. The cause of the ubiquitous finescale twinning is not clear. One may conjecture that it is the manifestation of concentration gradients at the mineralization front which in turn lead to anisotropic growth, local variations in the uptake of impurities and, consequently, stress concentrations which require a relief mechanism.

For the first time, the crystallographic relationships between third order lamellae, and adjacent first order lamellae have been determined, and again found to vary between species. In *O. sayana* the third order lamellae lie roughly parallel to the $(1\bar{1}0)$ planes,

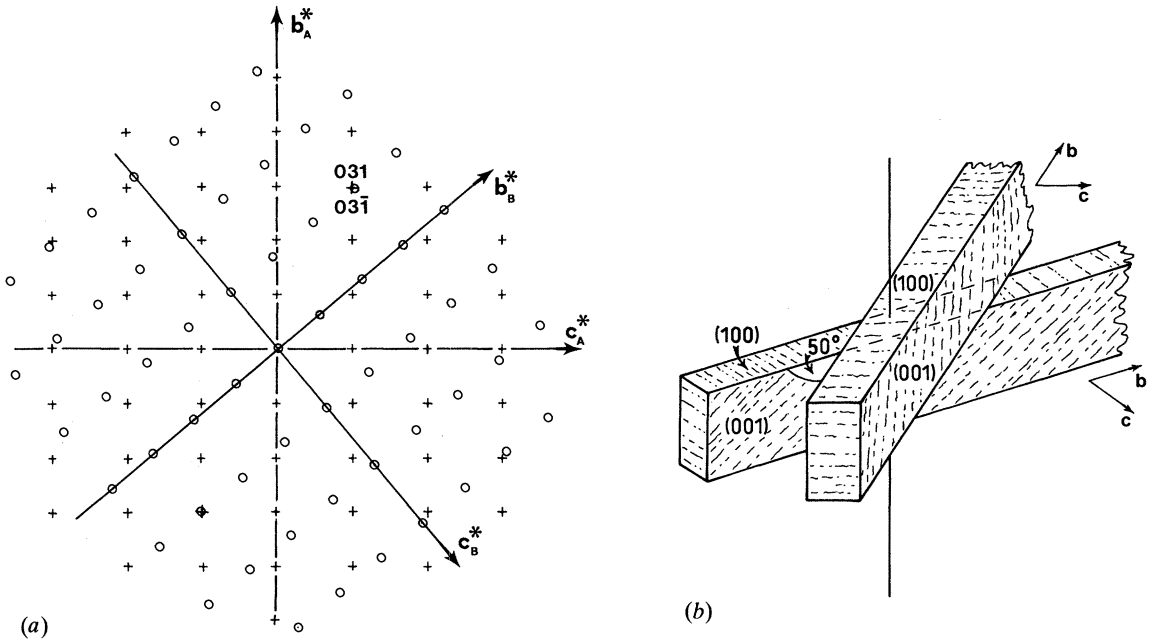

Figure 15. (*a*) Diagram of the inset SAD of figure 14*a*, produced by combining two [100] zone axis patterns, mutually rotated by approximately 50° around the [100] axis. The stars on the axes indicate that they are the axes of the reciprocal space lattices. The reflections from A-lamellae are represented by crosses, and those from B-lamellae are shown as open circles. (*b*) Sketch to illustrate the orientation relationship between two typical third order lamellae across a first order boundary in *Littorina littorea*. The lamellae cross-sections may differ from those shown schematically. The surfaces of the lamellae are shown as flat for reasons of simplicity; in practice they are probably stepped. The figure can be related directly with (*a*) since the cell axes b and c are parallel to the reciprocal lattice axes b* and c*.

rotating 45° around the normal to the twin plane across a first order boundary. In contrast, the third order lamellae of *L. littorea* show a sub-parallel alignment along [100], and a rotation of 50° across a first order boundary. The (001) plane appears as one of the two major lamellar surfaces in both cases.

These results emphasise the need for further studies of XLM crystallography to understand their full significance. The crystallographic variation found supports the view that crystal habit is controlled by the interlamellar matrix. It has been recognized that biomineralization is often an 'organic matrix-mediated' process (Lowenstam 1981), where the organic matter controls the nucleation, orientation, and size of the mineral, as well as influencing mechanical properties (Taylor & Layman 1972; Currey & Taylor 1974; Wainwright *et al.* 1976; Currey 1980; Krampitz *et al.* 1983; Wheeler & Sikes 1984, 1989; Addadi & Weiner 1989; Simkiss & Wilbur 1989; Laraia & Heuer 1990).

Many studies have been conducted to determine the structure and chemistry of such organic membranes. Investigations of the matrix composition of molluscan shells initially concentrated on whole shell analyses (Degans *et al.* 1967; Meenakshi *et al.* 1971), and found them to be species-specific. Later studies, concentrating on separate layers within a species indicate that matrix composition may be microstructure-specific (Haugen & Sejrup 1990; Samata 1990). Specific molecules involved in nucleation have been identified (Weiner 1983; Weiner *et al.* 1983; Weiner & Traub 1984), and two models of the nucleation process have been proposed: epitaxy, and ionotropy (see reviews by Mann 1983, 1988). 'Crystal engineering' has been recreated in the laboratory using Langmuir films (Mann & Heywood 1989; Mann *et al.* 1989; Mann 1990), establishing that such thin monolayers can control the type and orientation of calcium carbonate crystals generated.

The crystallographic relationships discovered in this study clearly demonstrate the importance of the interlamellar matrix in producing unique forms of XLM, and reveal the need for its more detailed investigation, such as performed on nacre (Weiner & Traub 1984). We find that the expression of the (001) face is present in both the forms of third order lamellae we have studied, as indeed it is in nacre. This suggests that the mineral-matrix interactions involved in nucleation in all cases may be closely related, but the extent and direction of growth perpendicular to [001] is variable.

The development of XLM is still unclear. Its macroscopic appearance might predispose one to anticipate that it is just a biogenic equivalent of epitaxial physical behaviour (the oriented overgrowth of one crystalline phase on the surface of another). However, the thin organic sheets that interleave the third order lamellae modify the precise epitaxial imperative that would otherwise apply. To date, only one detailed model of XLM secretion has been suggested (Nakahara *et al.* 1981). This proposes that third order lamellae develop within organic 'envelopes', beginning as small, randomly arranged crystals, and gradually elongating and becoming correctly orientated to form

PHILOSOPHICAL TRANSACTIONS OF THE ROYAL SOCIETY B BIOLOGICAL SCIENCES

mature XLM. This is supported by our SEM observations of XLM at growth surfaces. The minor species-specific variations of XLM, such as shape of third order lamellae (Haas 1972; Batten & Dumont 1976) and the presence or absence of second order lamellae, suggests further interspecific matrix and crystallographic differences to those that we have already identified. This would support the proposal that XLM has evolved independently several times (Taylor 1973; Batten 1982).

We are grateful for technical assistance from Mr C. G. Jones, Mr A. Whighton, Mr J. Spratt, and Mr K. Moulding. We also thank an anonymous referee for helpful comments.

REFERENCES

Addadi, L. & Weiner, S. 1989 Stereochemical and structural relations between macromolecules and crystals in biomineralization. In *Biomineralization. Chemical and biochemical perspectives* (ed. S. Mann, J. Webb & R. J. P. Williams), pp. 133–156. Weinheim, Germany: VCH Verlagsgesellschaft.

Bandel, K. 1979 Ubergänge von einfacheren Strukturtypen zur Kreuzlamellenstruktur bei Gastropodenschalen. *Biomin. Forsch Ber.* **10**, 9–38.

Bandel, K. 1990 Shell structure of the Gastropoda excluding Archaeogastropoda. In *Skeletal biomineralization: patterns, processes and evolutionary trends*, vol. 1 (ed. J. G. Carter), pp. 117–134. New York: Van Nostrand Reinhold.

Batten, R.L. 1982 The origin of gastropod shell structure. *Proc. Third N. Am. Paleont. Conv.* **1**, 35–39.

Batten, R.L. & Dumont, M.P. 1976 Shell ultrastructure of the Atlantidae (Heteropoda, Mesogastropoda) *Oxygyrus* and *Protatlanta*, with comments on *Atlanta inclinata*. *Bull. Am. Mus. nat. Hist.* **157**, 263–310.

Bøggild, O.B. 1930 The shell structure of the mollusks. *K. dansk. Vidensk. Selsk. Skr.* **2**, 232–325, pls. 1–15.

Burrage, B.J. & Pitkethly, D.R. 1969 Aragonite transformations observed in the electron microscope. *Phys. Stat. Solidi* **32**, 399–405.

Carter, J.G. 1990 Glossary of skeletal biomineralization. In *Skeletal biomineralization: patterns, processes and evolutionary trends*, vol. 1 (ed. J. G. Carter), pp. 609–627. New York: Van Nostrand Reinhold.

Carter, J.G. & Clark, G.R. 1985 Classification and phylogenetic significance of molluscan shell microstructure. In *Notes for a short course on mollusks* (ed. T. W. Broadhead) (Dept. Geol. Sci. Stud. Geol. **13**), pp. 50–71j. University of Tennessee.

Carter, J.G. & Lutz, R.A. 1990 Bivalvia (Mollusca). In *Skeletal biomineralization: patterns, processes and evolutionary trends*, vol. 2 (*Atlas and index*) (ed. J. G. Carter), pp. 5–28, pl. 1–121. New York: Van Nostrand Reinhold.

Currey, J.D. 1980 Mechanical properties of mollusc shell. *Symp. Soc. exp. Biol.* **34**, 75–97.

Currey, J.D. & Kohn, A.J. 1976 Fracture in the crossed-lamellar structure of *Conus* shells. *J. Mater. Sci.* **11**, 1616–1623.

Currey, J.D. & Taylor, J.D. 1974 The mechanical behaviour of some molluscan hard tissues. *J. Zool., Lond.* **173**, 395–406.

Degens, E.T., Spencer, D.W. & Parker, R.H. 1967 Palaeobiology of molluscan shell proteins. *Comp. Biochem. Physiol.* **20**, 553–579.

Grégoire, C. 1972 Structure of the molluscan shell. In *Chemical zoology*, vol. VII (*Mollusca*) (ed. M. Florkin & B. T. Scheer), pp. 45–102. New York, London: Academic Press.

Haas, W. 1972 Untersuchungen über die Mikro und Ultrastruktur der Polyplacophorenschale. *Biomin. Forsch Ber.* **5**, 1–52.

Haugen, J.E. & Sejrup, H.P. 1990 Amino acid composition of aragonitic conchiolin in the shell of *Arctica islandica*. *Lethaia* **23**, 133–141.

Kobayashi, I. 1964 Introduction to the shell structure of bivalvian molluscs. *Chikyù Kagaku*, **73**, 1–12.

Kobayashi, I. 1971 Internal shell microstructure of recent bivalvian molluscs. *Sci. Rep. Niigata Univ. Ser. E. Geol. Mineral.* **2**, 27–50, pl. 1–10.

Krampitz, G., Drolshagen, H., Häusle, J. & Hof-Irmscher, K. 1983 Organic matrices of mollusc shells. In *Biomineralization and biological metal accumulation* (ed. P. Westbroek & E. W. de Jong), pp. 231–247. Dordrecht: D. Reidel Publ. Co.

Laghi, G.F. & Russo, F. 1978 Struttura ed architettura delle piastre di *Chiton olivaceus* Spengler (Polyplacophora, Mollusca). *Boll. Soc. Paleont. Ital.* **17**, 272–291, pl. 1–7.

Laraia, V. & Heuer, A.H. 1990 Microstructure and mechanical behaviour of mollusk shells. *Proc. 11th Risø Int. Symp. Met. Mat. Sci.* pp. 79–96.

Laraia, V.J., Aindow, M. & Heuer, A.H. 1990 An electron microscopy study of the microstructure and microarchitecture of the *Strombus gigas* shell. *Mat. Res. Soc. Symp. Proc.* **174**, 117–124.

Lowenstam, H.A. 1981 Minerals formed by organisms. *Science, Wash.* **211**, 1126–1131.

MacClintock, C. 1967 Shell structure of patelloid and bellerophontoid gastropods (Mollusca). *Bull. Peabody Mus. nat. Hist.* **22**, 1–140.

Mann, S. 1983 Mineralization in biological systems. *Struct. Bond.* **54**, 125–174.

Mann, S. 1988 Molecular recognition in biomineralization. *Nature, Lond.* **332**, 119–124.

Mann, S. 1989 Crystallochemical strategies in biomineralization. In *Biomineralization, Chemical and biochemical perspectives* (ed. S. Mann, J. Webb & R. J. P. Williams), pp. 35–62. Weinheim, Germany: VCH Verlagsgesellschaft.

Mann, S. 1990 Crystal engineering: the natural way. *New Scient.* **125**(1707), 42–47.

Mann, S. & Heywood, B.R. 1989 Crystal engineering at interfaces. *Chem. Br.* 1989 (July), 698–700.

Mann, S., Heywood, B.R., Rajam, S. & Birchall, J.D. 1989 Interfacial control of nucleation of calcium carbonate under organized stearic acid monolayers. *Proc. R. Soc. Lond.* A**423**, 457–471.

McTigue, J.W., Jr. & Wenk, H.R. 1985 Microstructures and orientation relationships in the dry-state aragonite-calcite and calcite-lime phase transformations. *Am. Mineral.* **70**, 1253–1261.

Meenakshi, V.R., Hare, P.E. & Wilbur, K.M. 1971 Amino acids of the organic matrix of neogastropod shells. *Comp. Biochem. Physiol.* **40B**, 1037–1043.

Nakahara, H., Kakei, M. & Bevelander, G. 1981 Studies on the formation of the crossed lamellar structure in the shell of *Strombus gigas*. *Veliger*, **23**, 207–211.

Ness, S.E., Haywick, D.W. & Cuff, C. 1990 High-resolution transmission electron microscopy of biogenic aragonite. *Mineral Mag.* **54**, 589–592.

Runnegar, B. 1984 Crystallography of the foliated calcite shell layers of bivalve molluscs. *Alcheringa*, **8**, 273–290.

Samata, T. 1990 Ca-binding glycoproteins in molluscan shells with different types of ultrastructure. *Veliger* **33**, 190–201.

PHILOSOPHICAL TRANSACTIONS OF THE ROYAL SOCIETY B BIOLOGICAL SCIENCES

Shimamoto, M. 1986 Shell microstructure of the Veneridae (Bivalvia) and its phylogenetic implications. *Tohoku Univ. Sci. Rep.*, 2nd ser. (*Geol.*), **56**, 1–39, pl. 1–20.

Simkiss, K. & Wilbur, K.M. 1989 *Biomineralization: cell biology and mineral deposition.* (xiv + 337 pages.) San Diego: Academic Press.

Taylor, J.D. 1973 The structural evolution of the bivalve shell. *Palaeontology* **16**, 519–534.

Taylor, J.D., Kennedy, W.J. & Hall, A. 1969 The shell structure and mineralogy of the Bivalvia. Introduction. Nuculacea—Trigonacea. *Bull. Br. Mus. nat. Hist. Zool. Suppl.* **3**, 1–125, 29 pl.

Taylor, J.D., Kennedy, W.J. & Hall A. 1973 The shell structure and mineralogy of the Bivalvia. II. Lucinacea—Clavagellacea. Conclusions. *Bull. Br. Mus. nat. Hist. Zool.* **22**(9), 253–294, 15 pl.

Taylor, J.D. & Layman, M. 1972 The mechanical properties of bivalve (Mollusca) shell structures. *Palaeontology* **15**, 73–87.

Taylor, J.D. & Reid, D.G. 1990 Shell microstructure and mineralogy of the Littorinidae: ecological and evolutionary significance. *Hydrobiologia* **193**, 199–215.

Towe, K.M. & Thompson, G.R. 1972 The structure of some bivalve shell carbonates prepared by ion-beam thinning. A comparison study. *Calc. Tiss. Res.* **10**, 38–48.

Uozumi, S., Iwata, K. & Togo, Y. 1972 The ultrastructure of the mineral and the construction of the crossed-lamellar layer in molluscan shell. *J. Fac. Sci. Hokkaido Univ. ser. IV*, **15**, 447–478.

Wainwright, S.A., Biggs, W.D., Currey, J.D. & Gosline, J.M. 1976 *Mechanical design in organisms.* (423 pages.) London: Edward Arnold.

Watabe, N. 1984 Mollusca: Shell. In *Biology of the integument*, vol. I (*Invertebrates*) (ed. J. Bereiter-Hahn, K. Matoltsy & S. K. Richards), pp. 448–485. New York: Springer-Verlag.

Weiner, S. 1983 Molusc shell formation: Isolation of two organic matrix proteins associated with calcite deposition in the bivalve *Mytilus californianus*. *Biochemistry* **22**, 4139–4144.

Weiner, S., Talmon, Y. & Traub, W. 1983 Electron diffraction of mollusk shell organic matrices and their relationship to the mineral phase. *Int. J. Biol. Macromol.* **5**, 325–328.

Weiner, S. & Traub, W. 1984 Macromolecules in mollusc shells and their functions in biomineralization. *Phil. Trans. R. Soc. Lond.* B, **304**, 425–434.

Wheeler, A.P. & Sikes, C.S. 1984 Regulation of carbonate calcification by organic matrix. *Am. Zool*, **24**, 933–944.

Wheeler, A.P. & Sikes, C.S. 1989 Matrix-crystal interactions in calcium carbonate biomineralization. In *Biomineralization. Chemical and biochemical perspectives*. (ed. S. Mann, J. Webb & R. J. P. Williams). pp. 95–131. Weinheim, West Germany: VCH Verlagsgesellschaft.

Wilbur, K.M. & Saleuddin, A.S.M. 1983 Shell formation. In *The Mollusca*, vol. 4 (*Physiology Part 1*) (ed. A. S. M. Saleuddin & K. M. Wilbur), pp. 235–287. New York, London: Academic Press.

Williams, R.C. & Fisher, H.W. 1970 Electron microscopy of tobacco mosaic virus under conditions of minimal beam exposure. *J. molec. Biol.* **52**, 121–123.

Wise, S.W. 1971 Shell ultrastructure of the taxodont pelecypod *Anadara notabilis* (Röding). *Eclogae geol. Helv.* **64**, 1–12, pl. I–IX.

Zischke, J.A., Watabe, N. & Wilbur, K.M. 1970 Studies on shell formation: measurement of growth in the gastropod *Ampullarius glaucus*. *Malacologia*, **10**, 423–439.

Received 11 November 1991; revised and accepted 14 February 1992

PHILOSOPHICAL TRANSACTIONS OF THE ROYAL SOCIETY B BIOLOGICAL SCIENCES

PHILOSOPHICAL TRANSACTIONS OF THE ROYAL SOCIETY B BIOLOGICAL SCIENCES

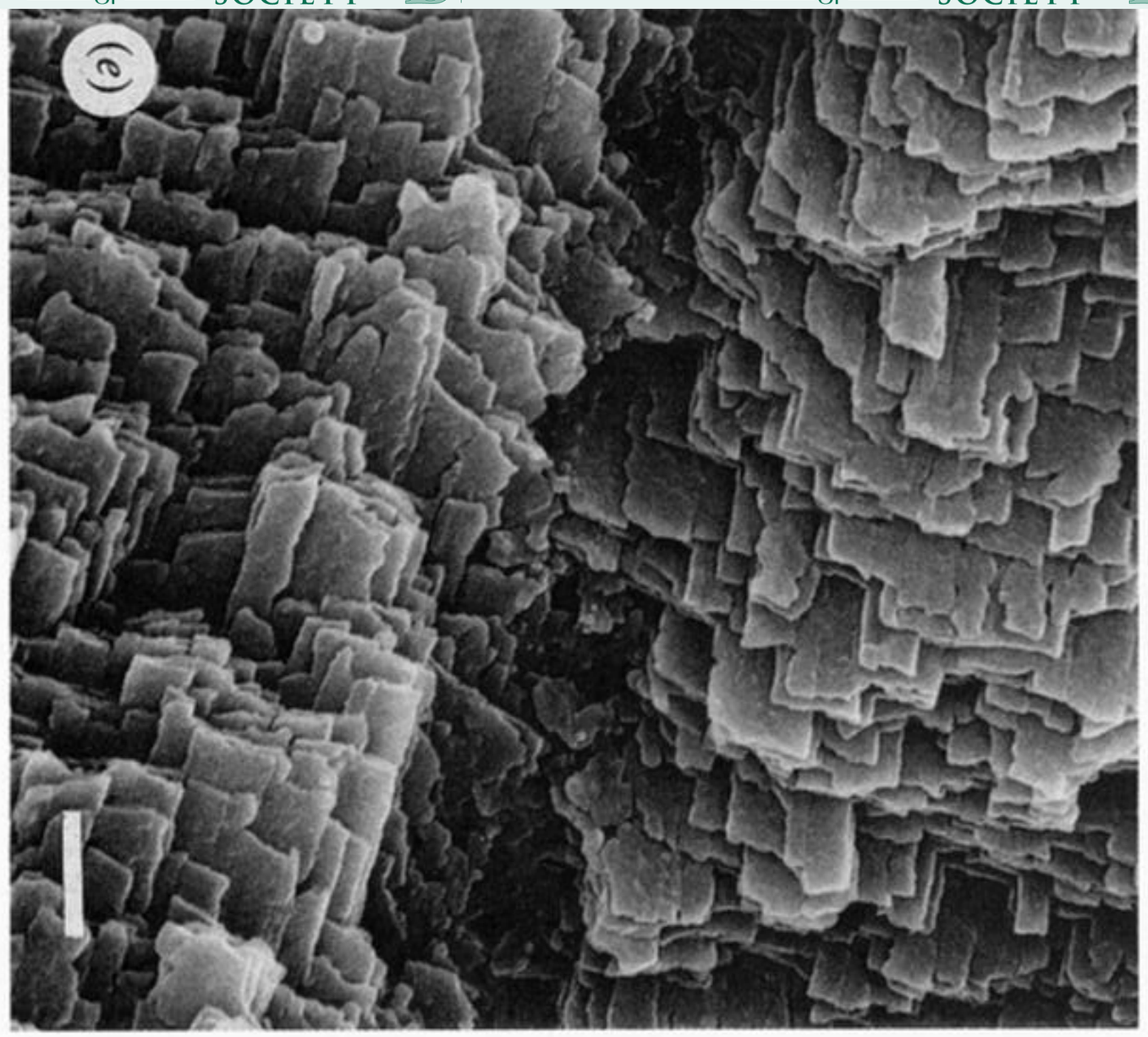

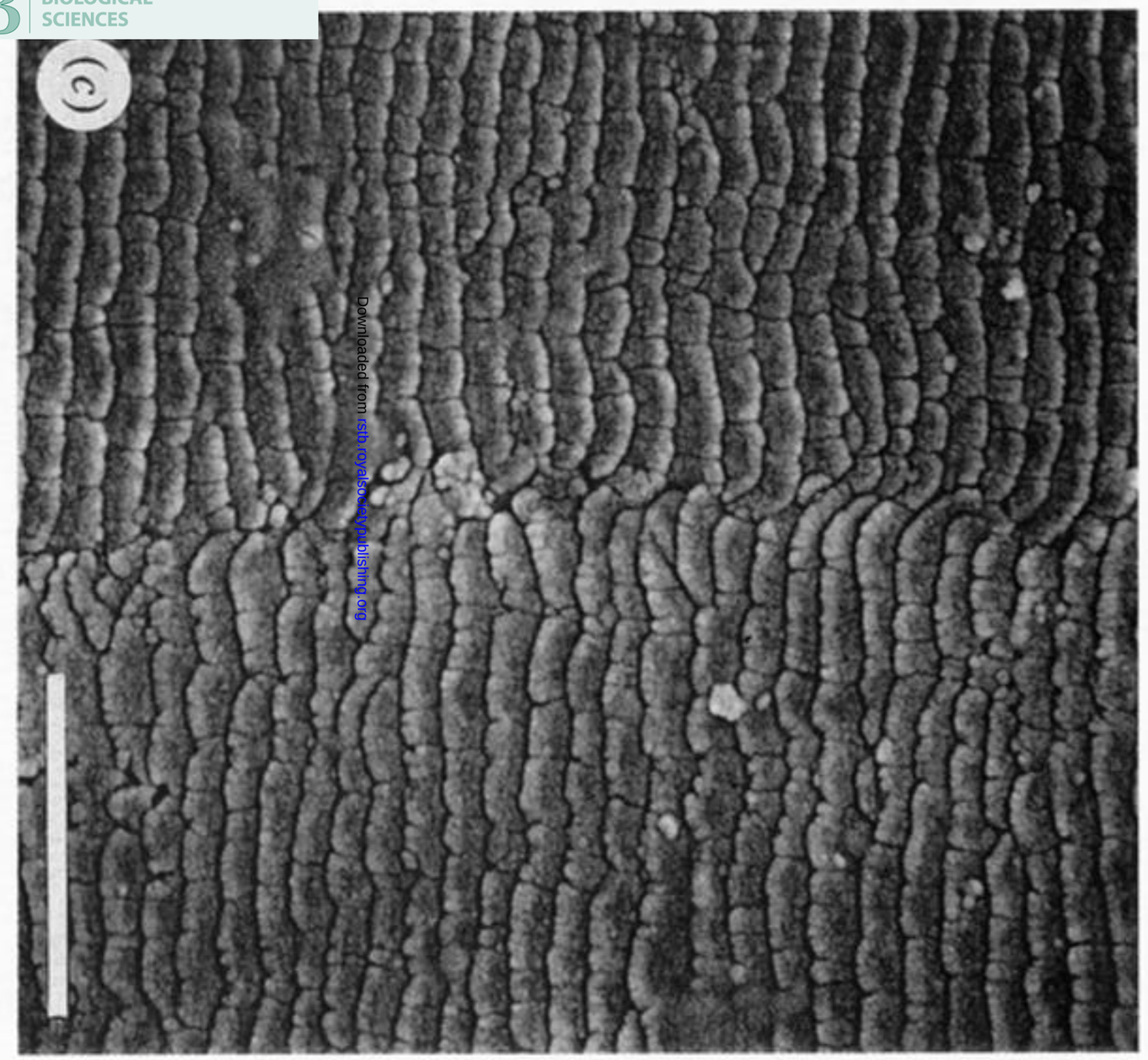

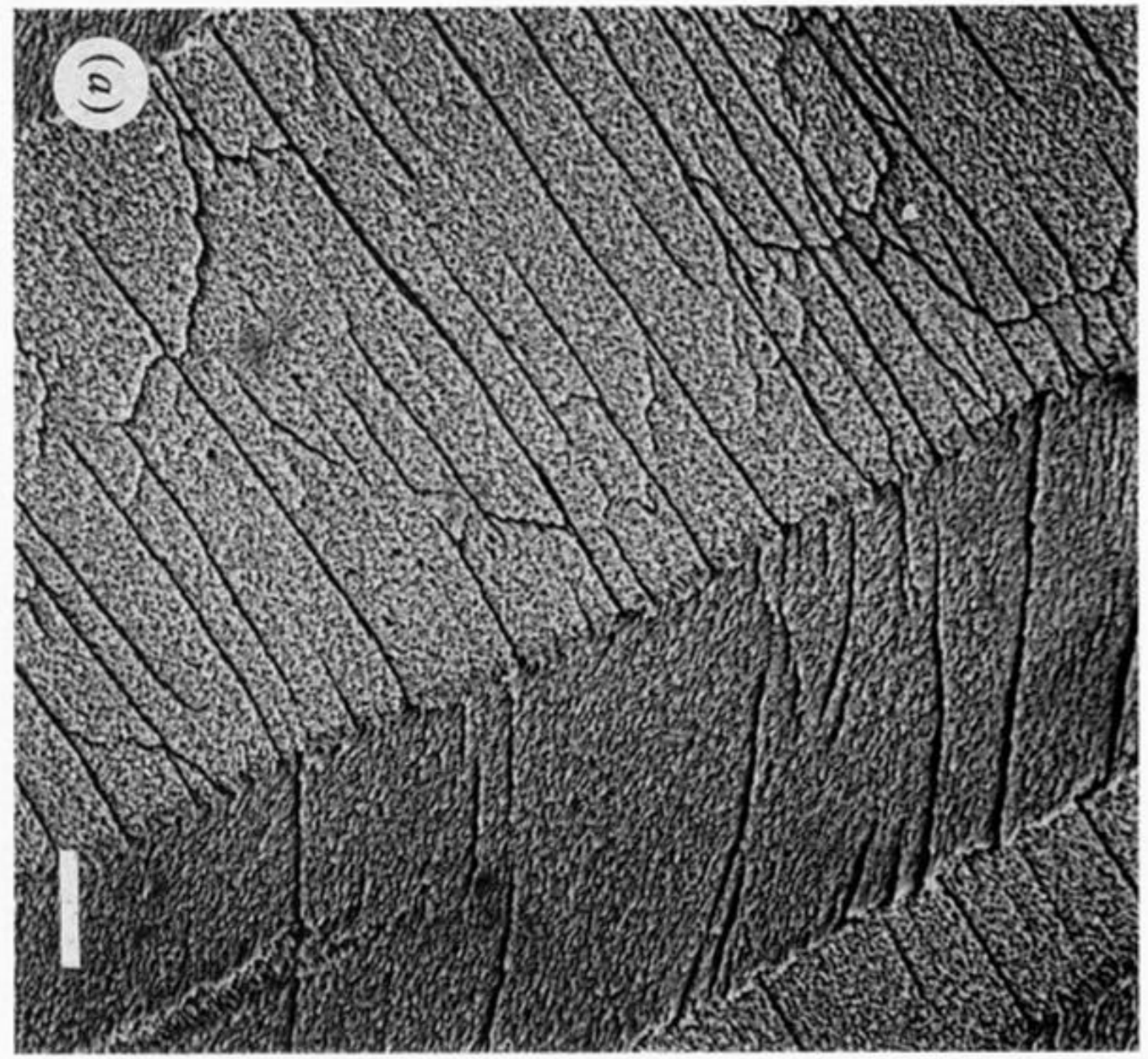

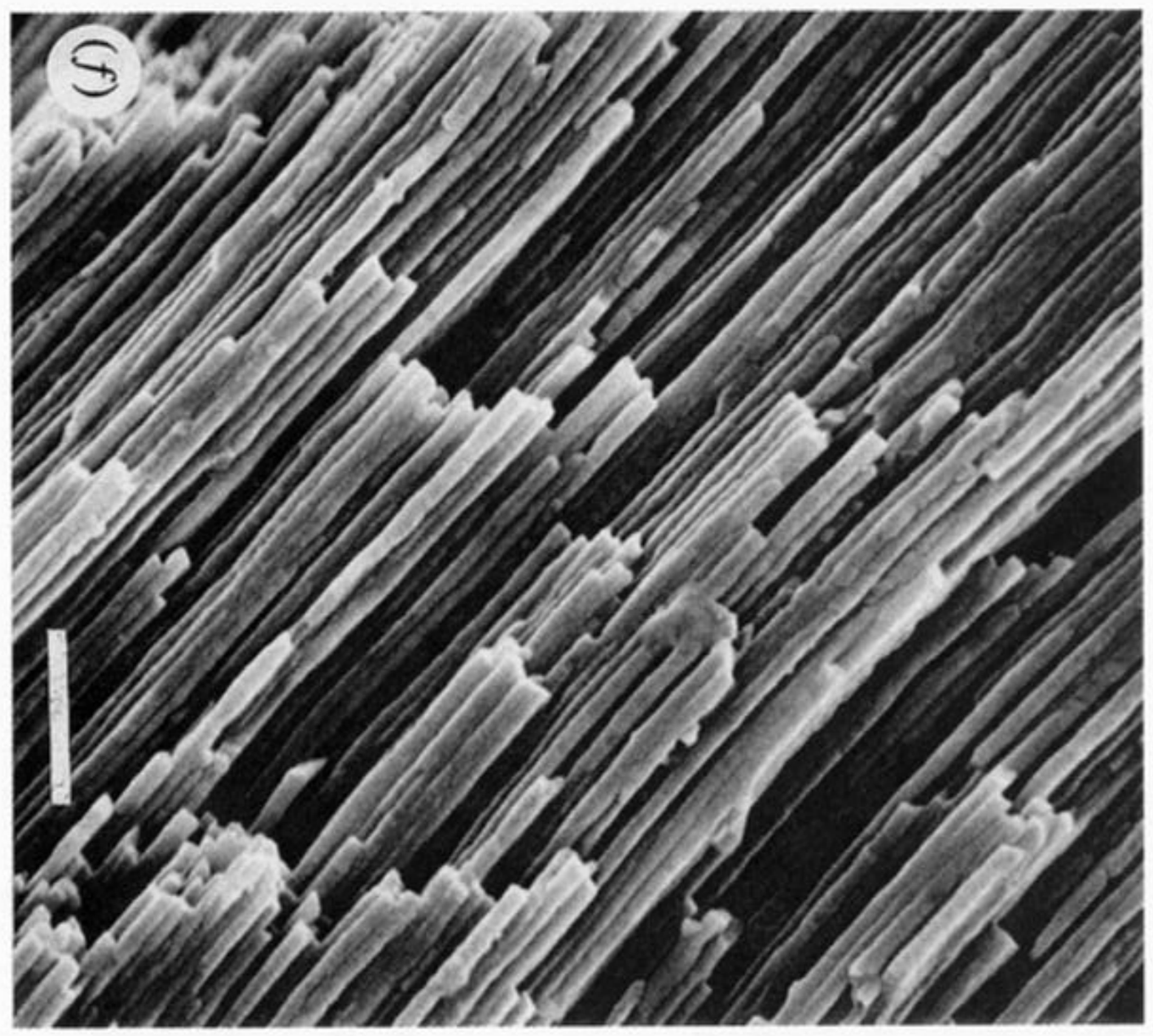

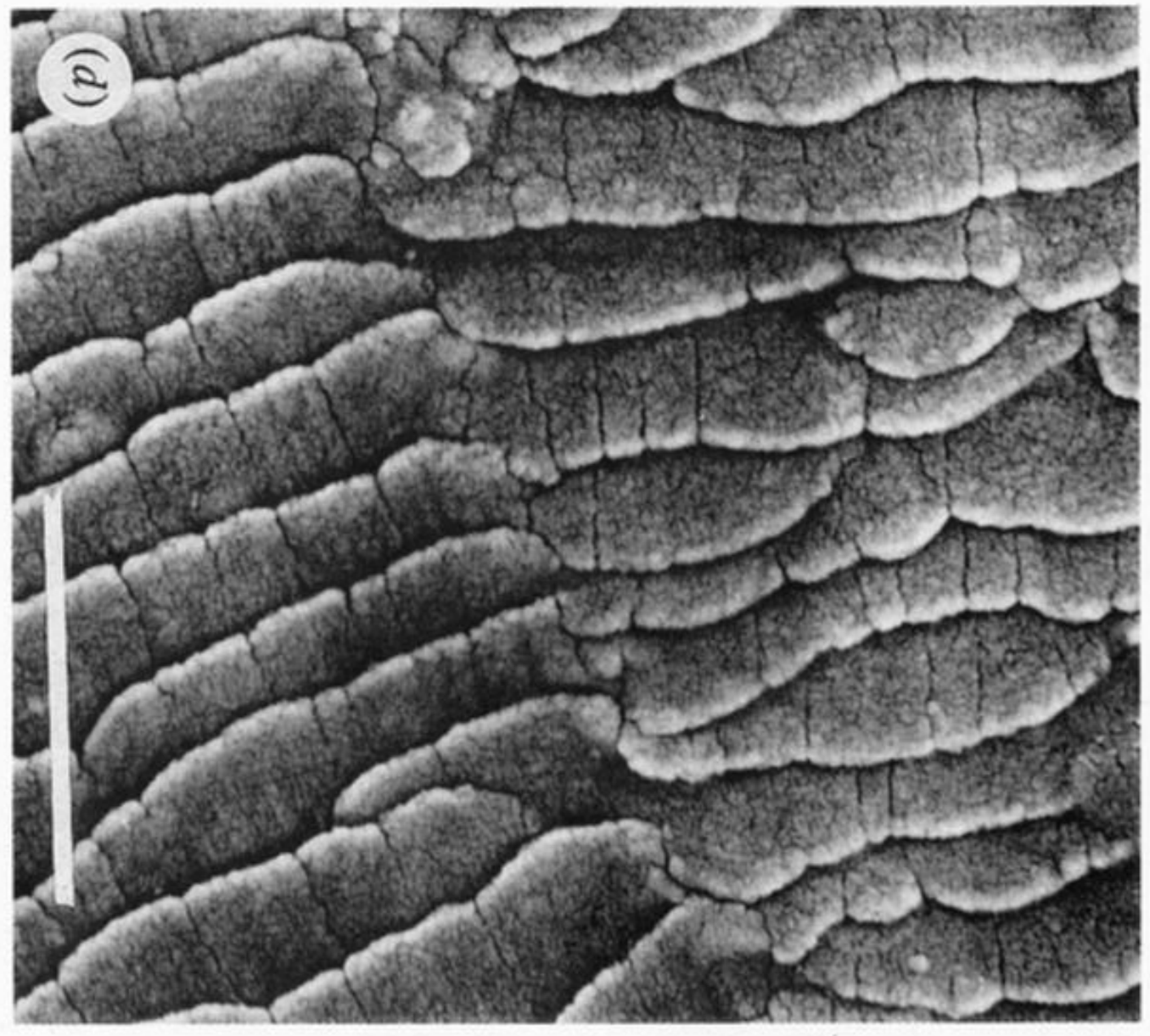

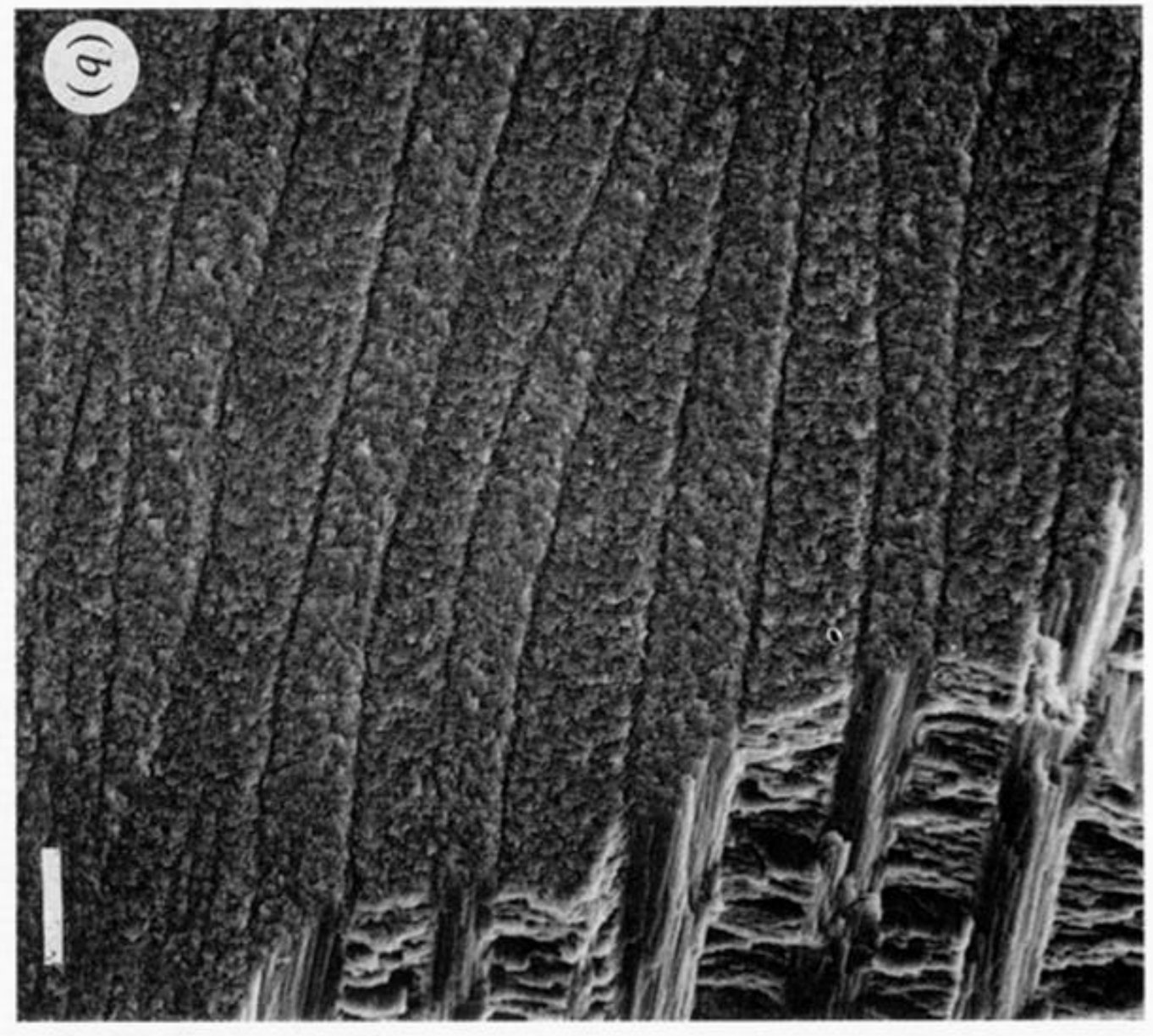

Figure 2.

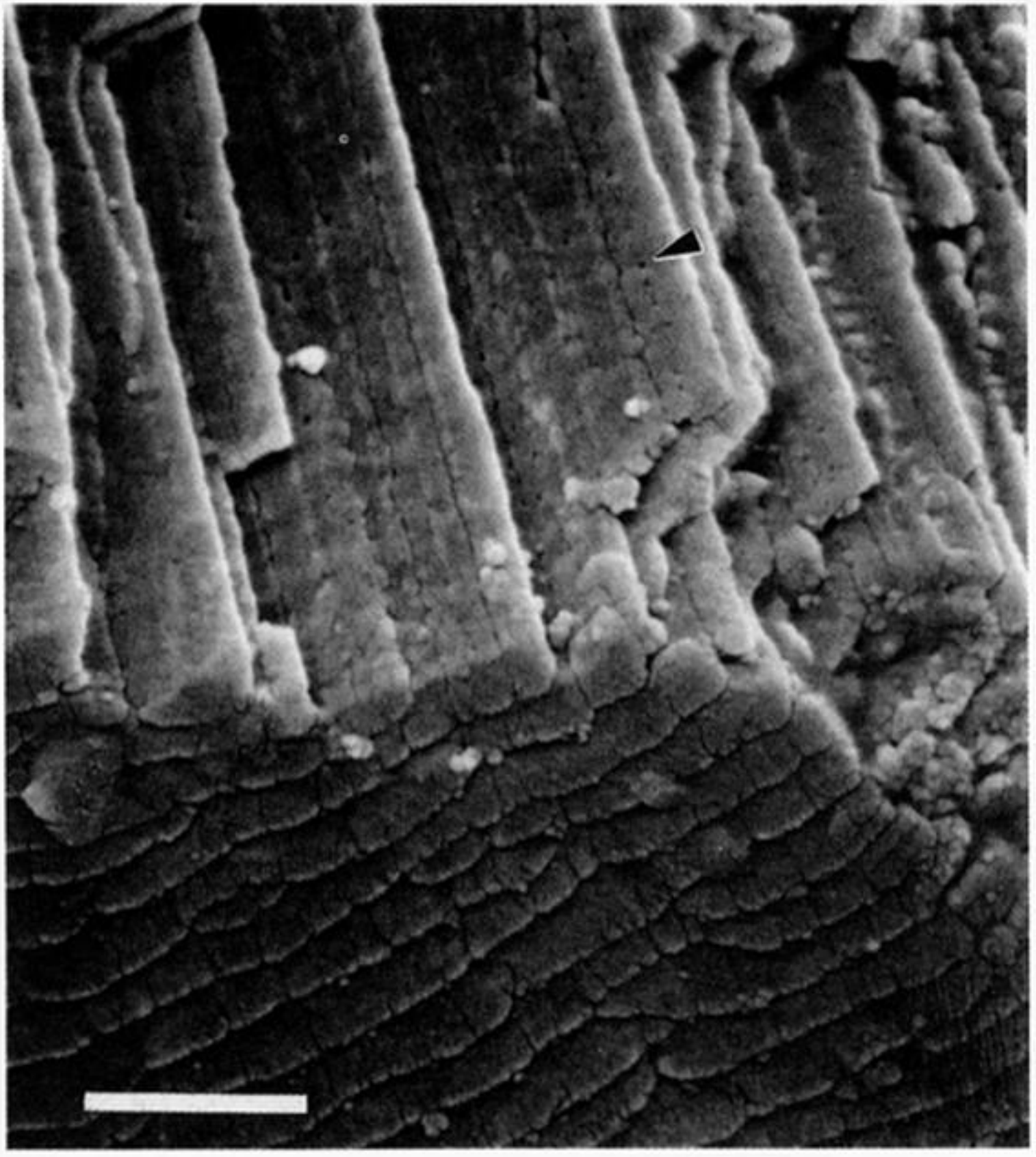

gure 3. Pits on third order lamellae, exposed on fracture rfaces of *Patella vulgata*. Note the difference between the tual width of third order lamellae as seen on the fracture rface, compared with their apparent width on the growth rface. Scale bar = 1 μm.

PHILOSOPHICAL TRANSACTIONS OF THE ROYAL SOCIETY B BIOLOGICAL SCIENCES

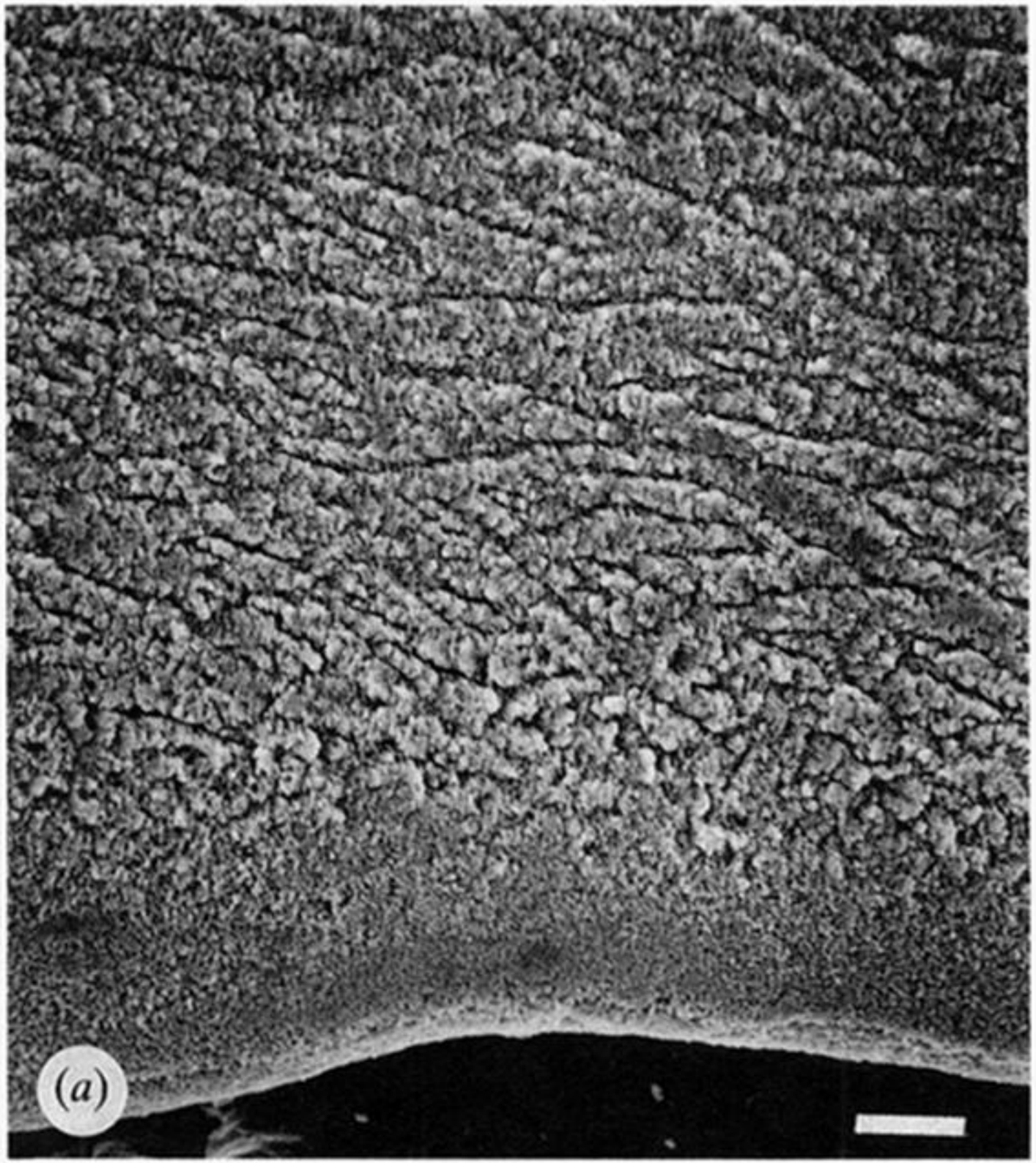

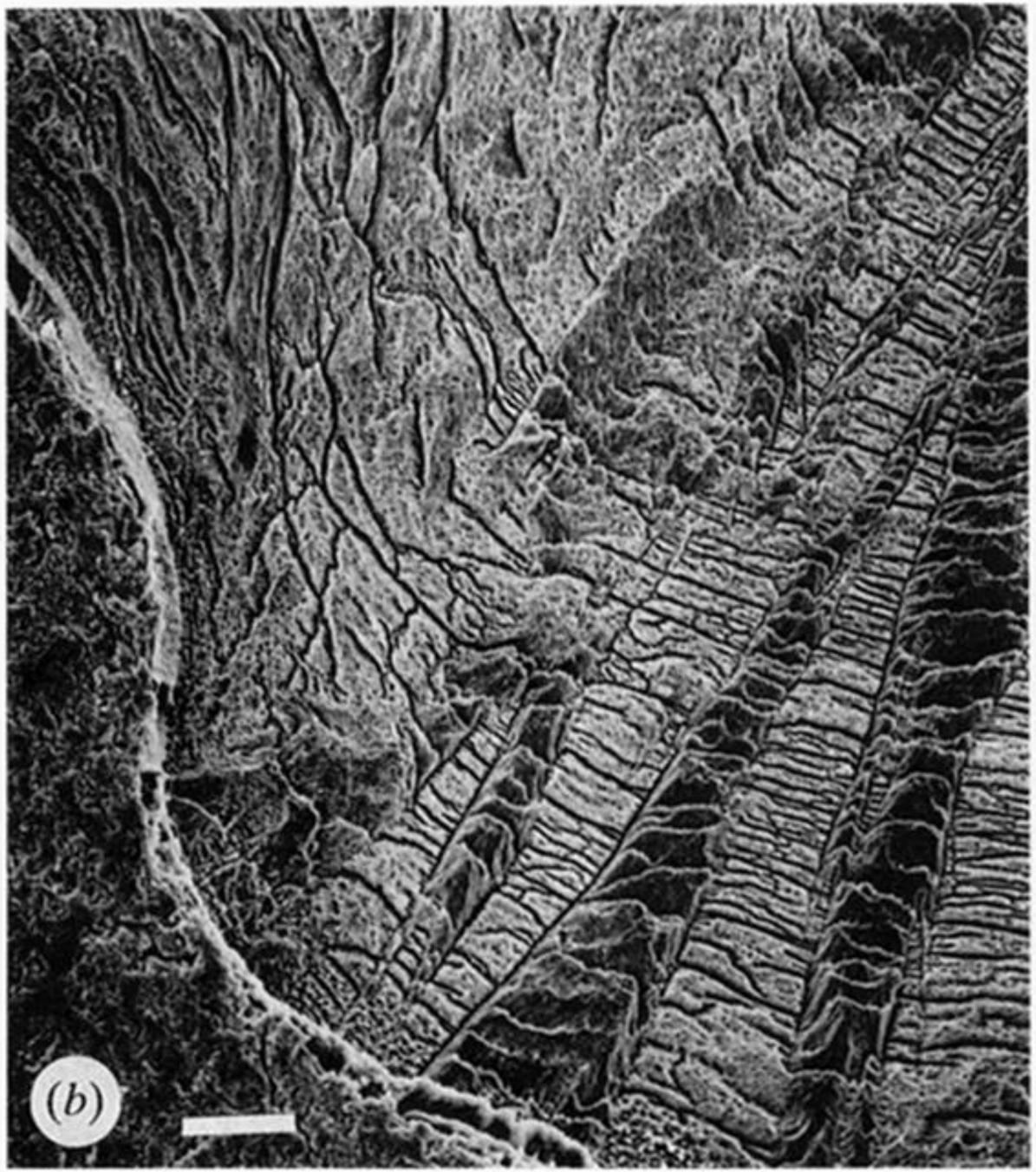

gure 4. Margins of the shell growth surface of *Arca tetragona*. (*a*) Surface view showing a progression from fine mogeneous structure to more ordered first order lamellae. Eventually, regular first order lamellae are generated, in figure 2*b*. Scale bar = 20 μm. (*b*) Etched radial section through the growth surface, with disorganized crystals ading into XLM. Scale bar = 20 μm.

PHILOSOPHICAL TRANSACTIONS OF THE ROYAL SOCIETY B BIOLOGICAL SCIENCES

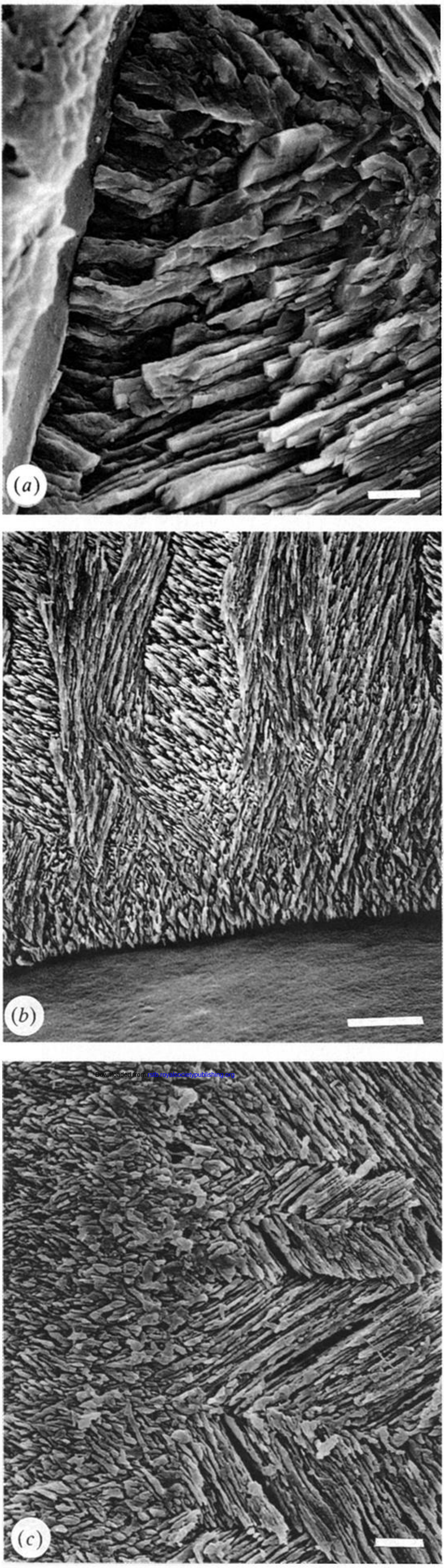

igure 5 (*a*) *Oliva sayana*. Transverse section showing initial ystals lying perpendicular to the shell surface. Scale ar = 1 μm. (*b*) *Conus magus*. Etched radial section through ie shell. Third order lamellae secreted directly onto the eriostracum (bottom) are not initially organized into first der lamellae. Scale bar = 5 μm. (*c*) *Pomatias elegans*. Etched dial section showing gradual transition to XLM. Scale ar = 2 μm.

gure 6. Etched radial section of *Conus magus* showing the boundary between two XLM layers. Scale bar = 20 μm.

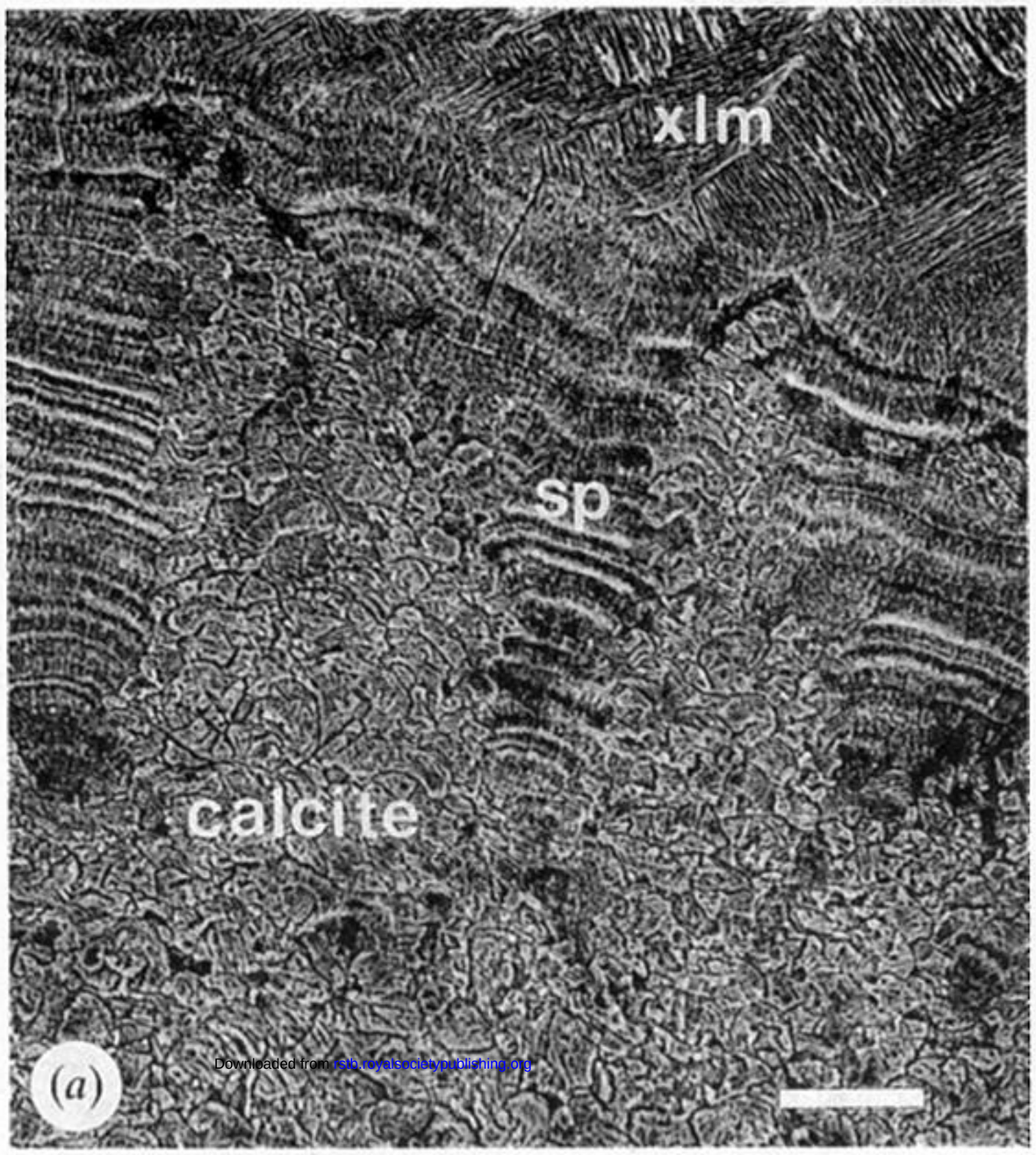

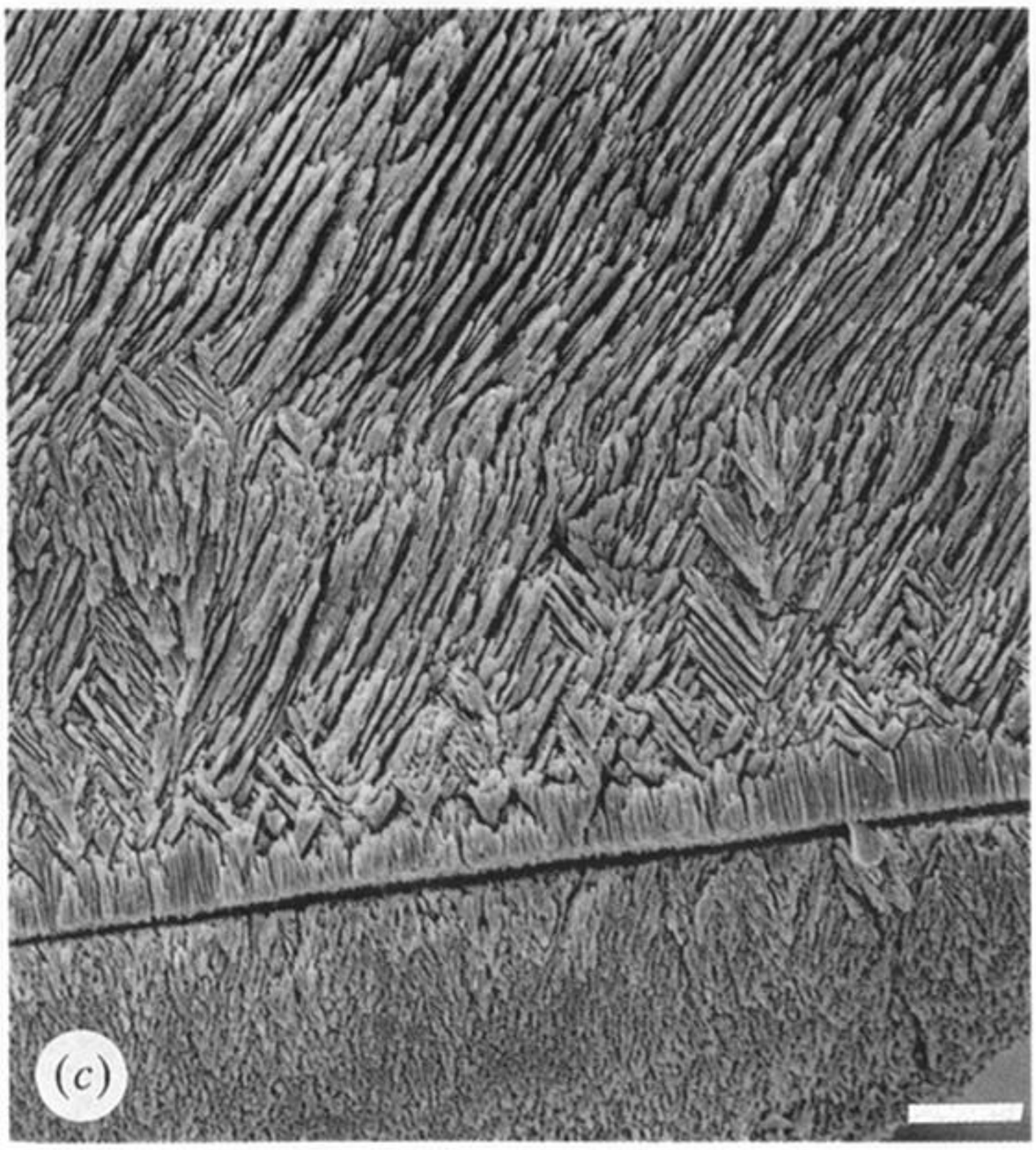

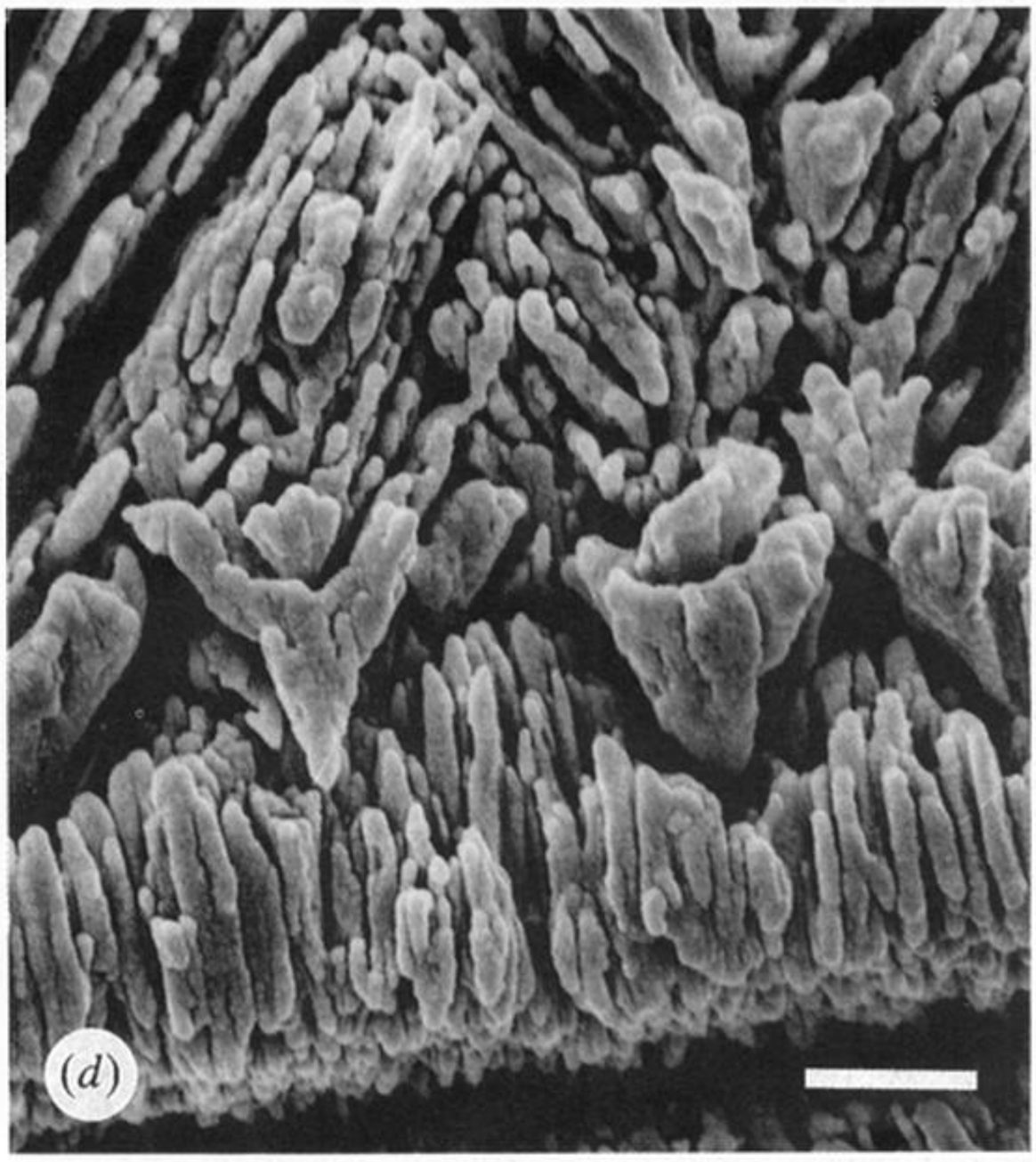

igure 7. XLM preceded by a spherulitic layer. (*a*) *Neptunea antiqua*. Irregular cavities in blocky calcite (bottom) are led by spherulitic structure (sp), which grades into XLM (top). Scale bar = 20 μm. (*b–d*) *Pomatias elegans*. pherulitic-prismatic layer (bottom), overlain by XLM. (*b*) Etched radial section. Scale bar = 2 μm. (*c*) Well-defined yer of acicular crystals at the spherulite–XLM boundary marked by a line in the lower half of the photograph. Scale ar = 4 μm. (*d*) Close up of acicular crystals in (*c*). Scale bar = 1 μm.

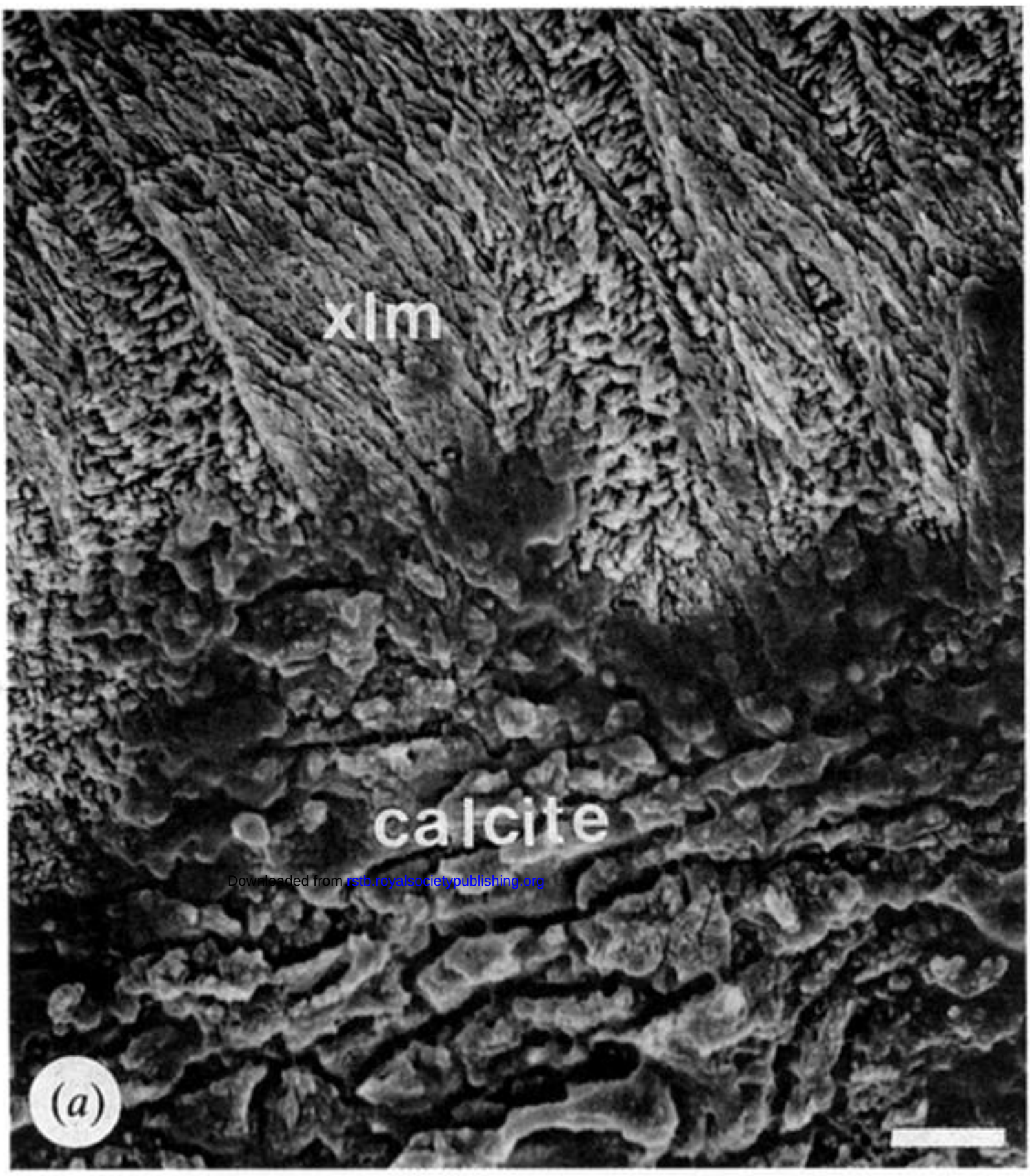

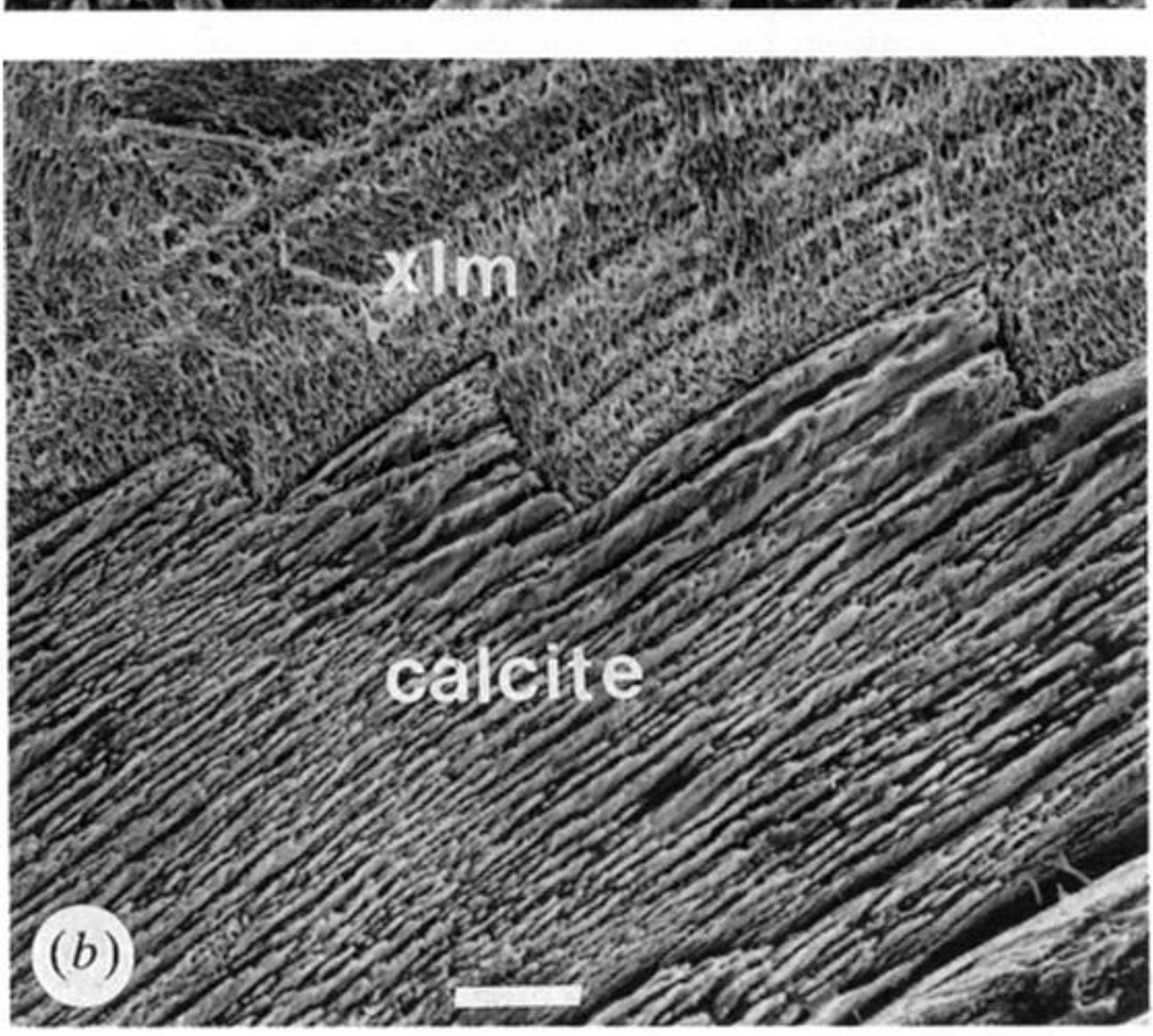

igure 8. Abrupt, irregular junctions between calcite micro-ructures and XLM. (*a*) *Littorina littorea*. Note the concentra-on of darker organic matter at the boundary between ocky calcite (below) and XLM (above). Scale bar = 4 μm.) *Patella vulgata*. Aragonitic XLM above, calcitic crossed-liated structure below. Scale bar = 10 μm.

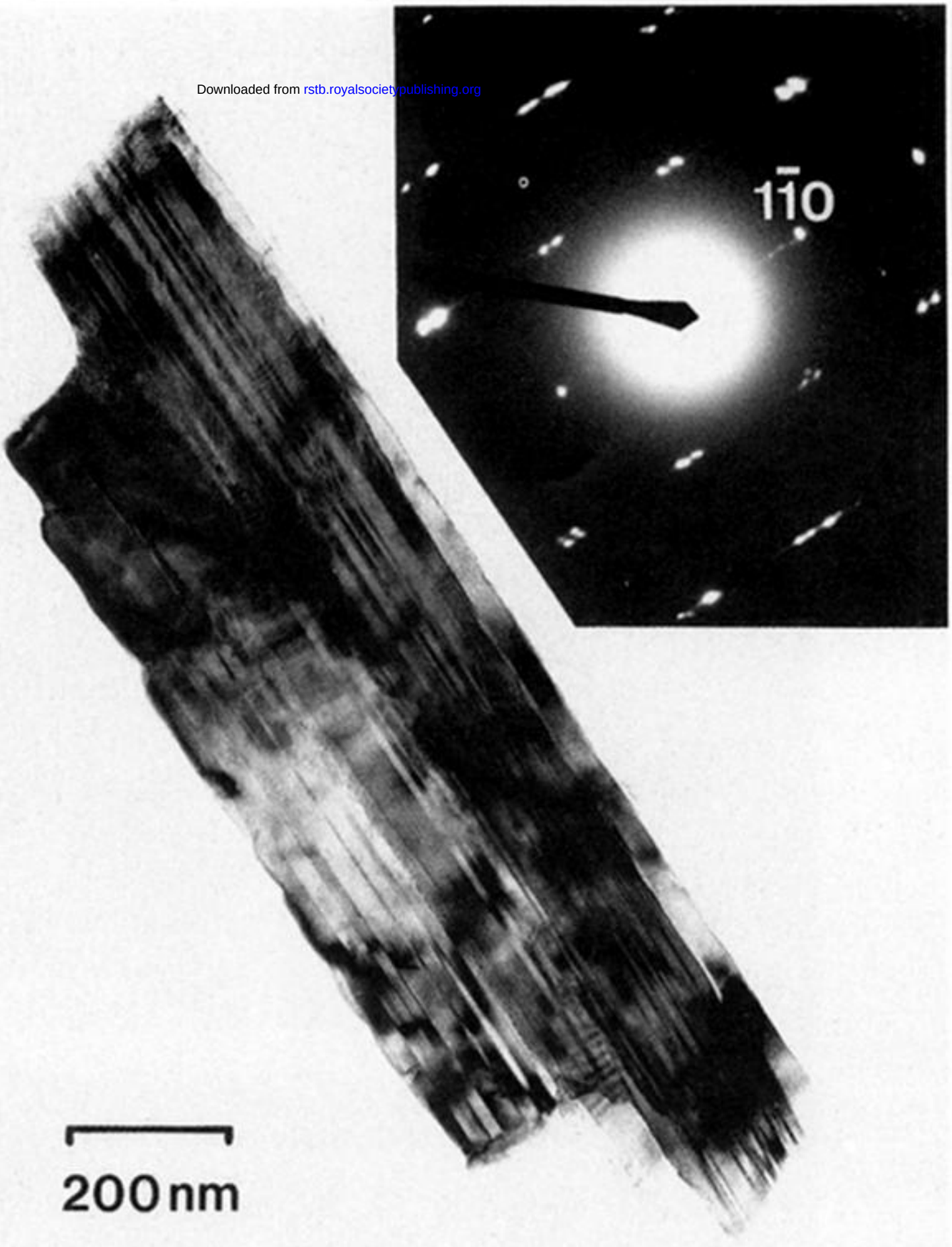

gure 9. TEM image showing fragment of a single third der lamella from *Oliva sayana*, with multiple (1$\bar{1}$0) twinning and corresponding [001] zone axis diffraction pattern nset).

PHILOSOPHICAL TRANSACTIONS OF THE ROYAL SOCIETY B BIOLOGICAL SCIENCES

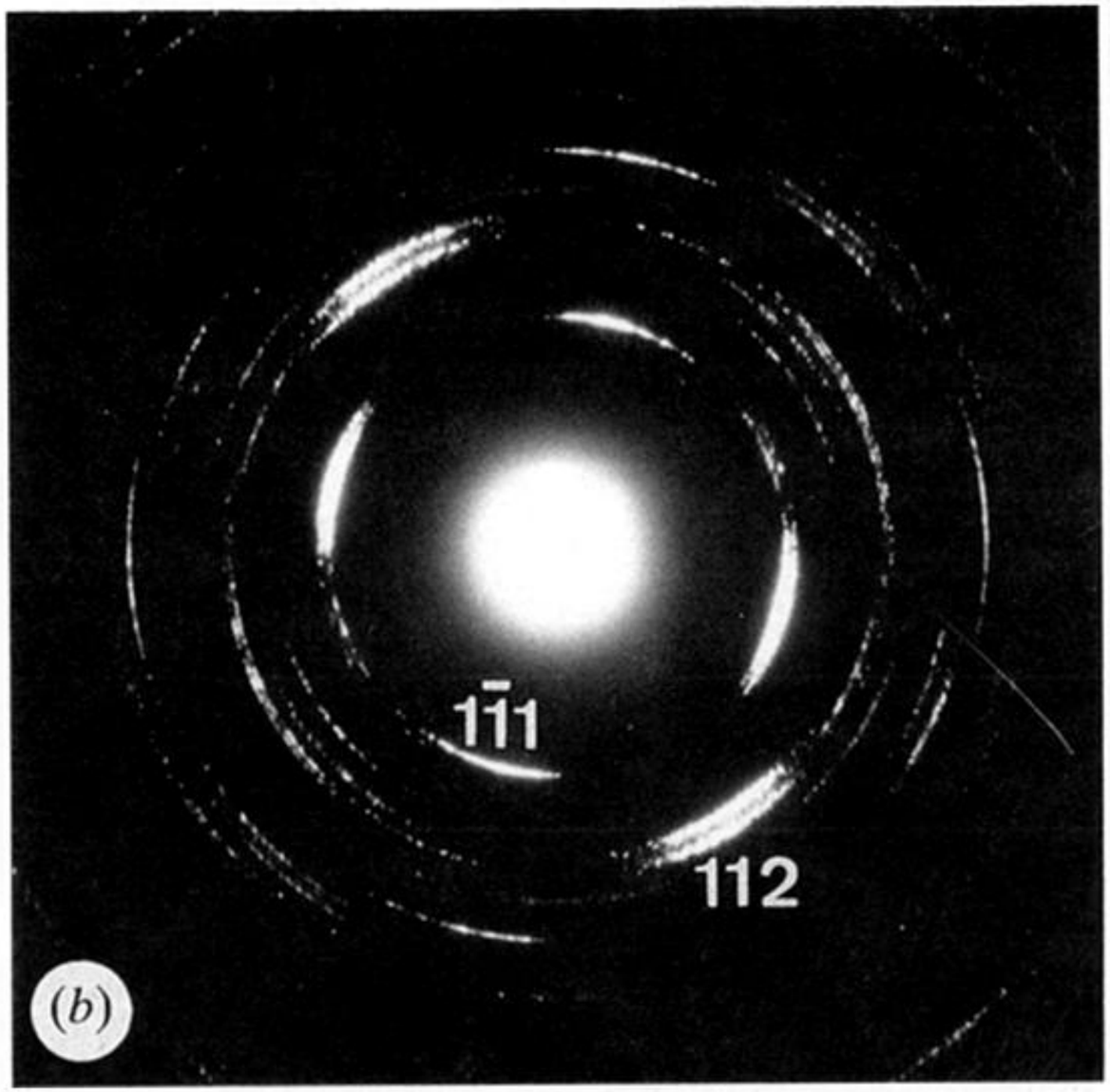

gure 10. *Oliva sayana*. (*a*) TEM image of the boundary zone between first order lamellae, with one set of third der lamellae approximately 'end-on' and the other 'side-on'. Note the approximate parallelism of (1$\bar{1}$0) twinning ross the boundary zone, although a few third order lamellae right at the boundary are strongly misorientated.) [31$\bar{2}$] zone axis diffraction pattern from 'end-on' third order lamellae in (*a*), showing strong texture.

PHILOSOPHICAL TRANSACTIONS OF THE ROYAL SOCIETY B BIOLOGICAL SCIENCES

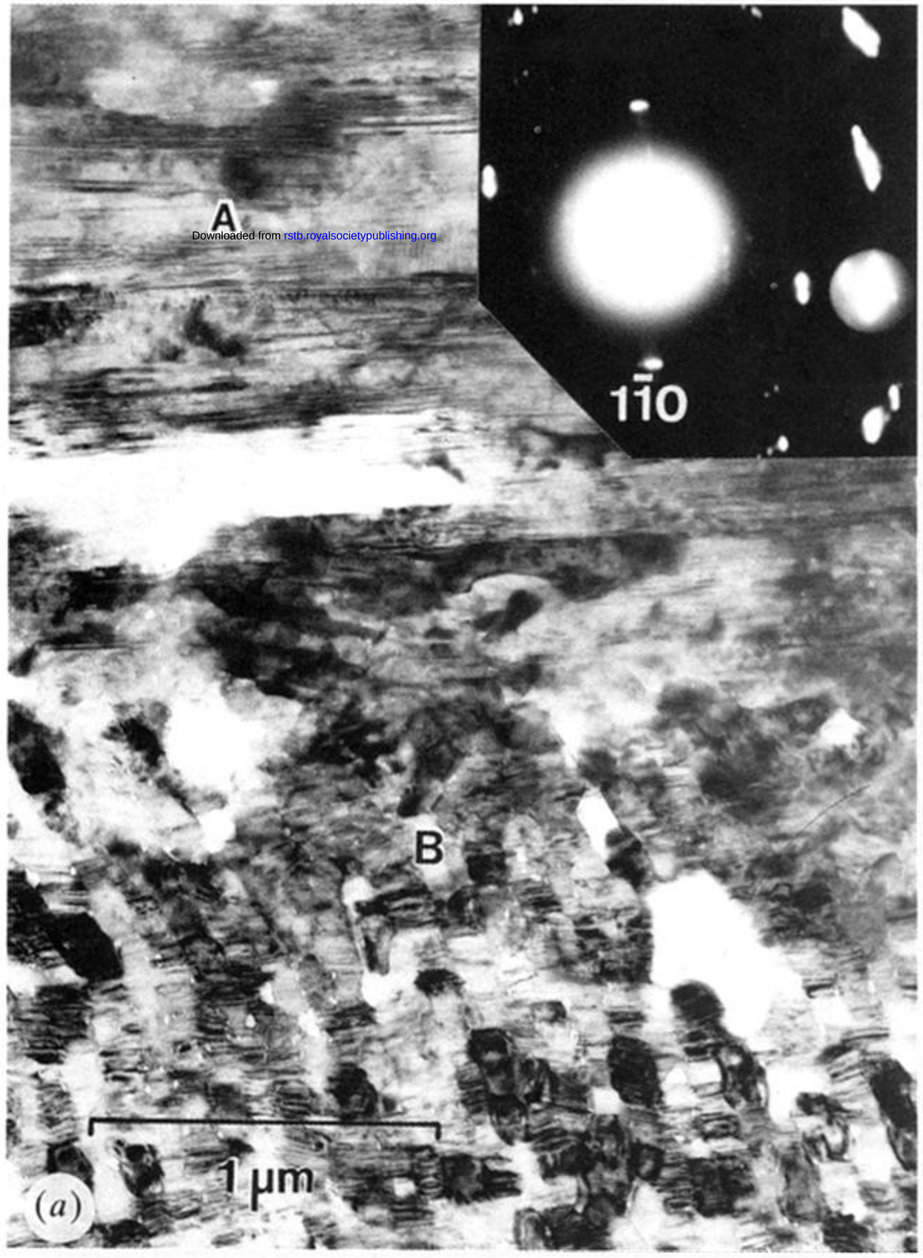

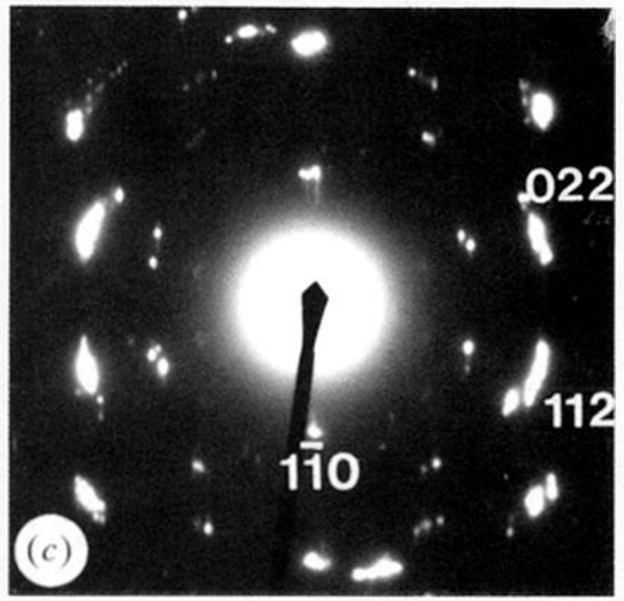

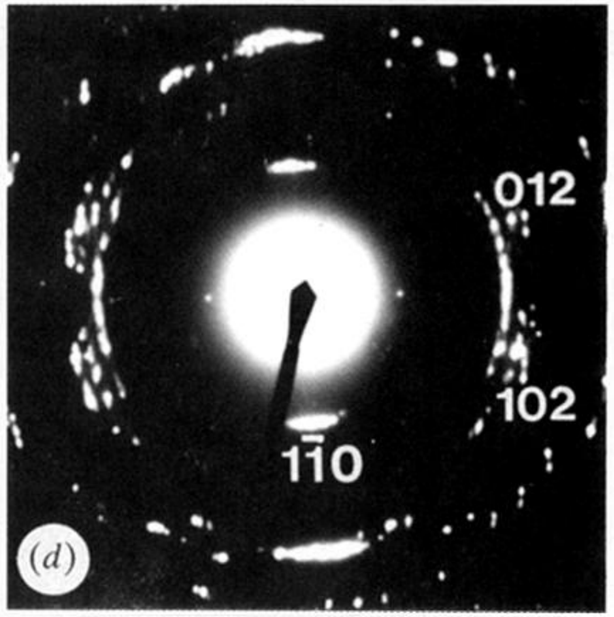

igure 11. *Oliva sayana*. (*a*) Bright field TEM image of first order boundary zone and (inset) superposed selected area diffraction pattern (SAD) from the zone. Note (110) winning and some porosity. (*b*) Centred dark field TEM image corresponding to (*a*), recorded with the objective aperture positioned around the almost coincident 112 and 02 reflections (from third order lamellae), as indicated in the inset of (*a*). (*c*) [11$\bar{1}$] zone axis SAD, with minor arcing of reflections, from field near (A) in (*a*). (*d*) [22$\bar{1}$] zone xis SAD, with strong arcing of relections, from field centred on (B) in (*a*).

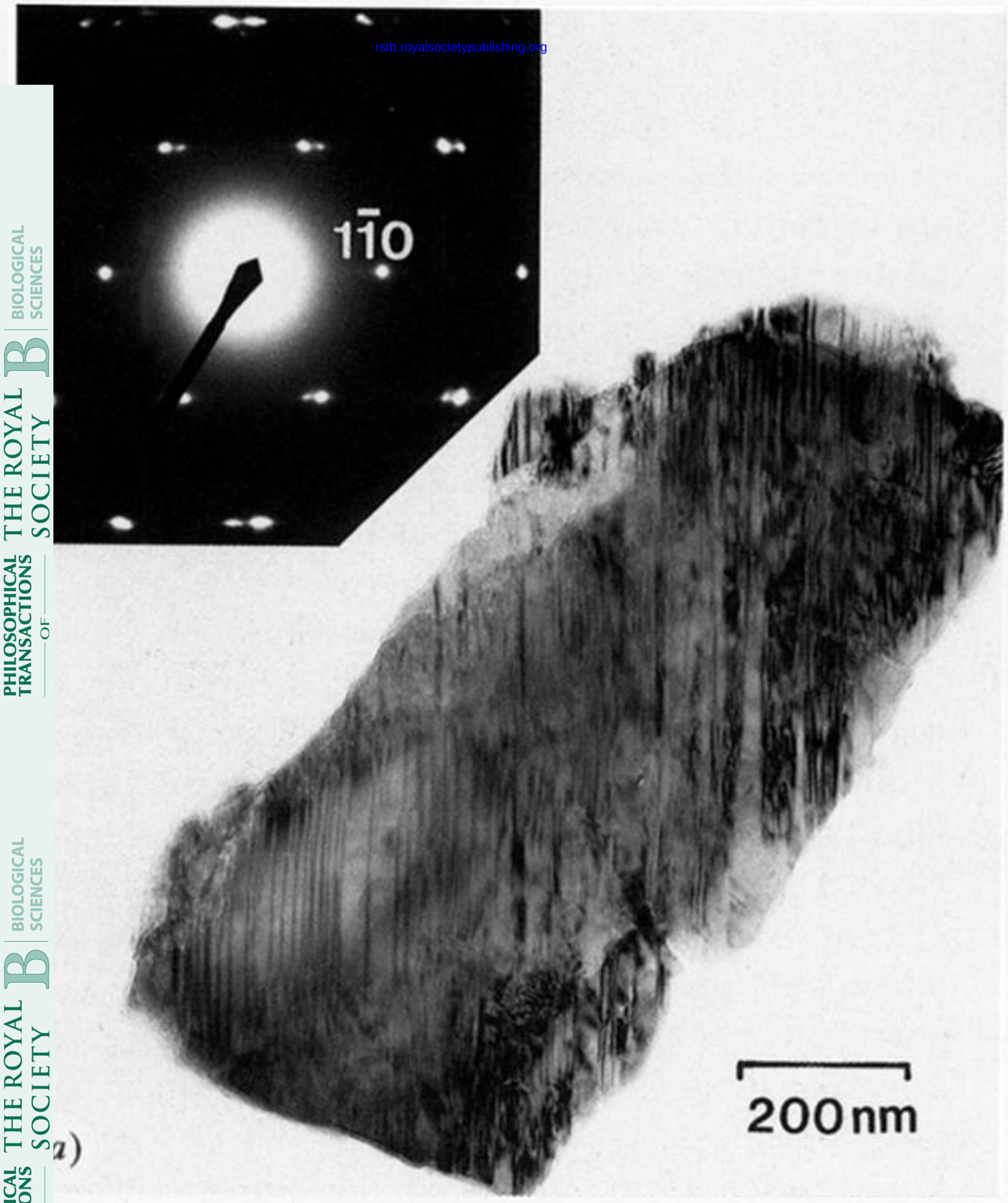

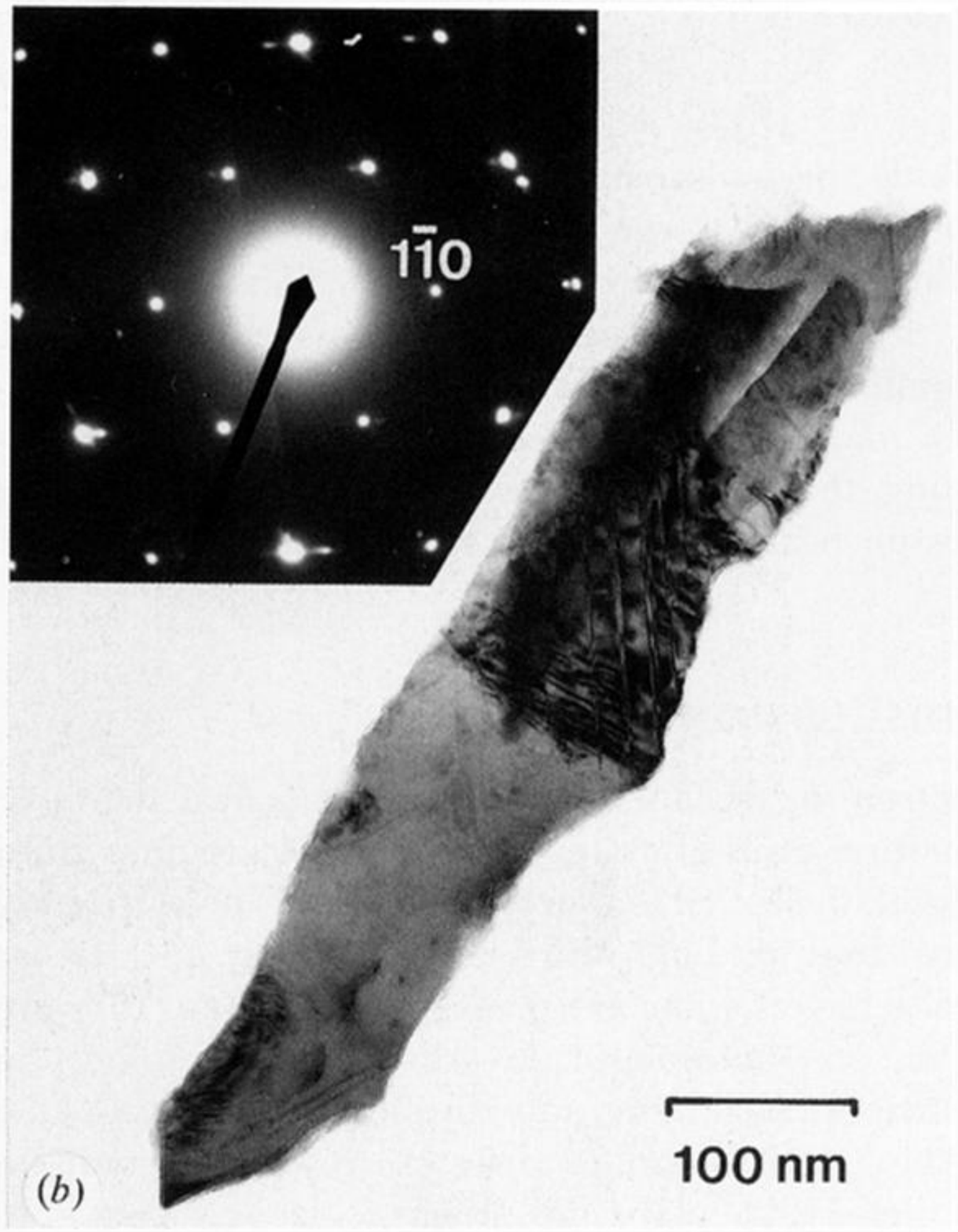

gure 13. (*a*) TEM image of fragment of a single third order lamella from *Littorina littorea*, with multiple (1$\bar{1}$0) winning and corresponding [001] zone axis diffraction pattern (inset). (*b*) TEM image of another fragment of a gle third order lamella from *L. littorea*, showing both (1$\bar{1}$0) and (110) twinning, and with corresponding [001] ne axis diffraction pattern (inset).

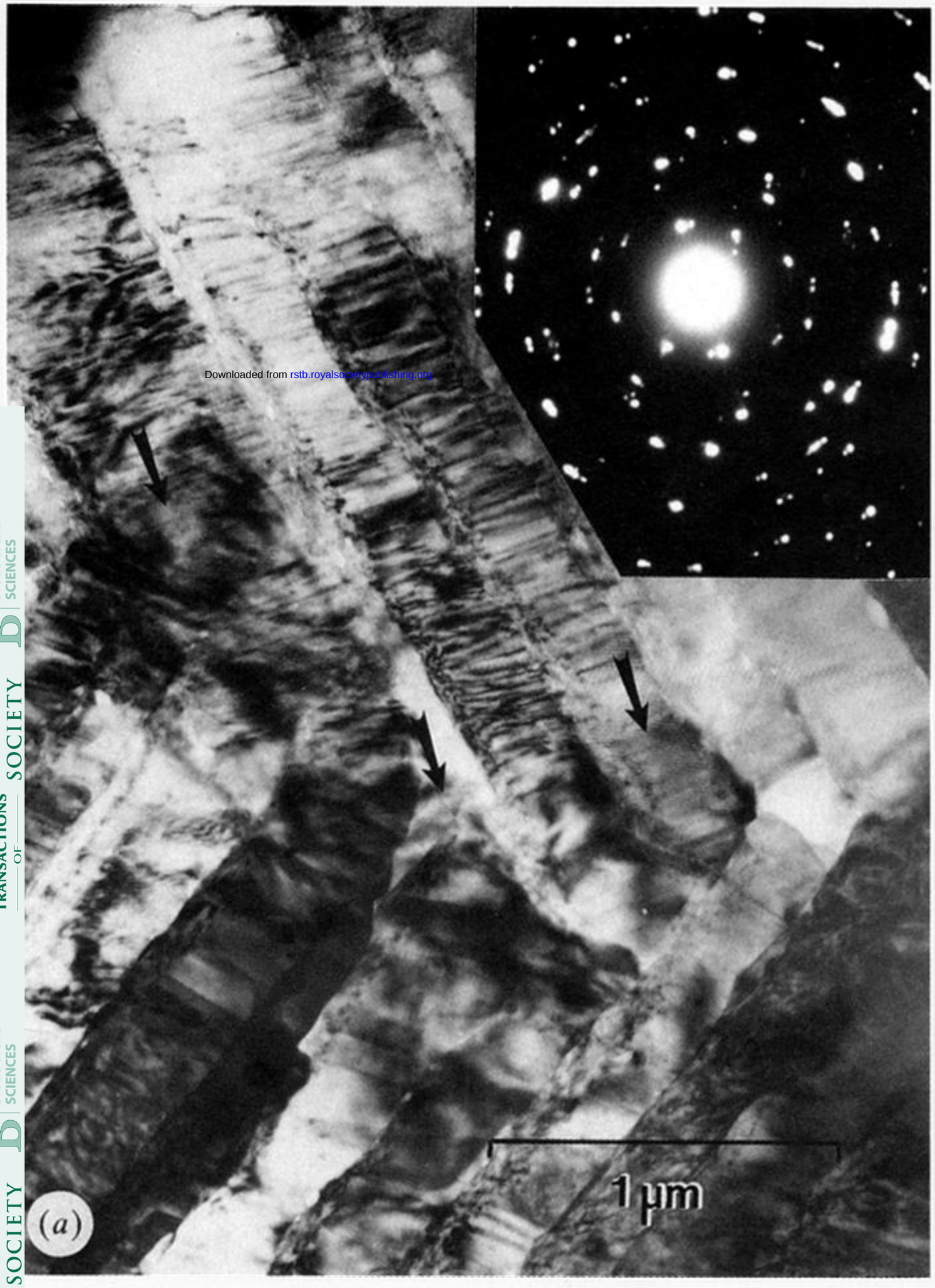

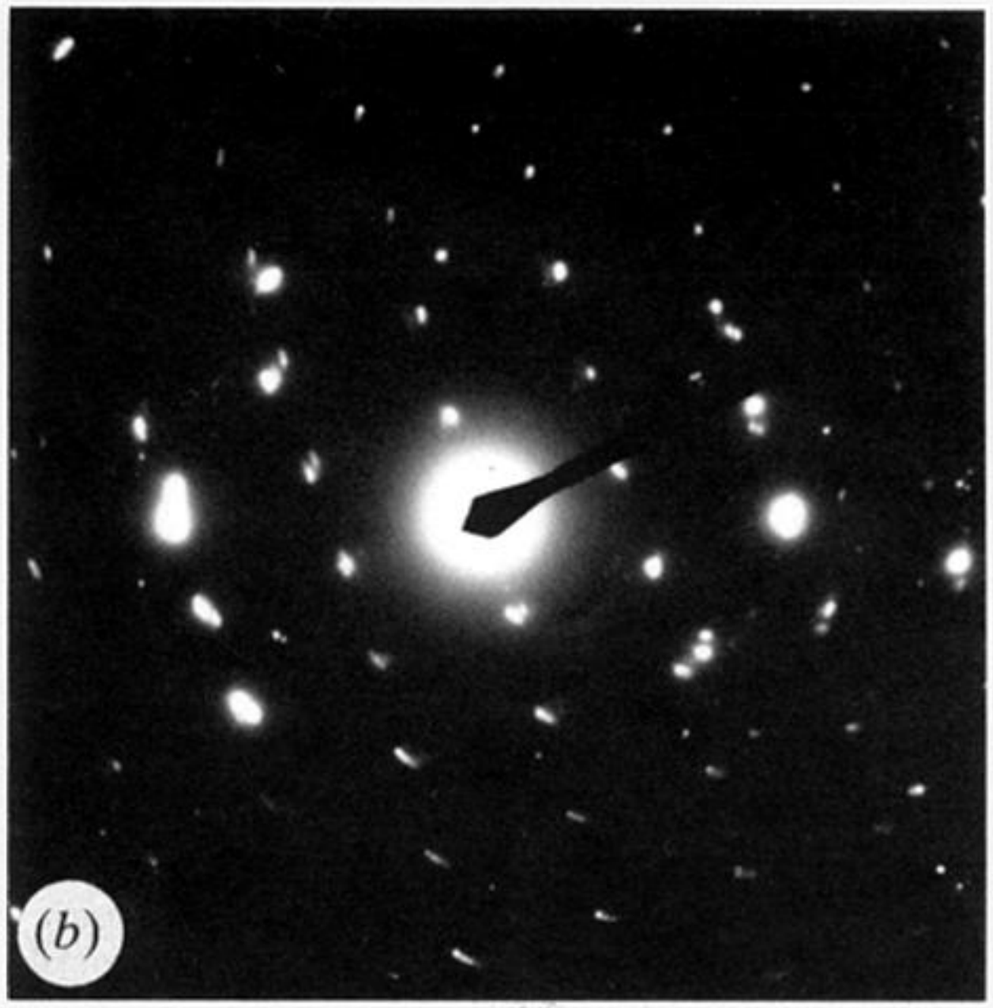

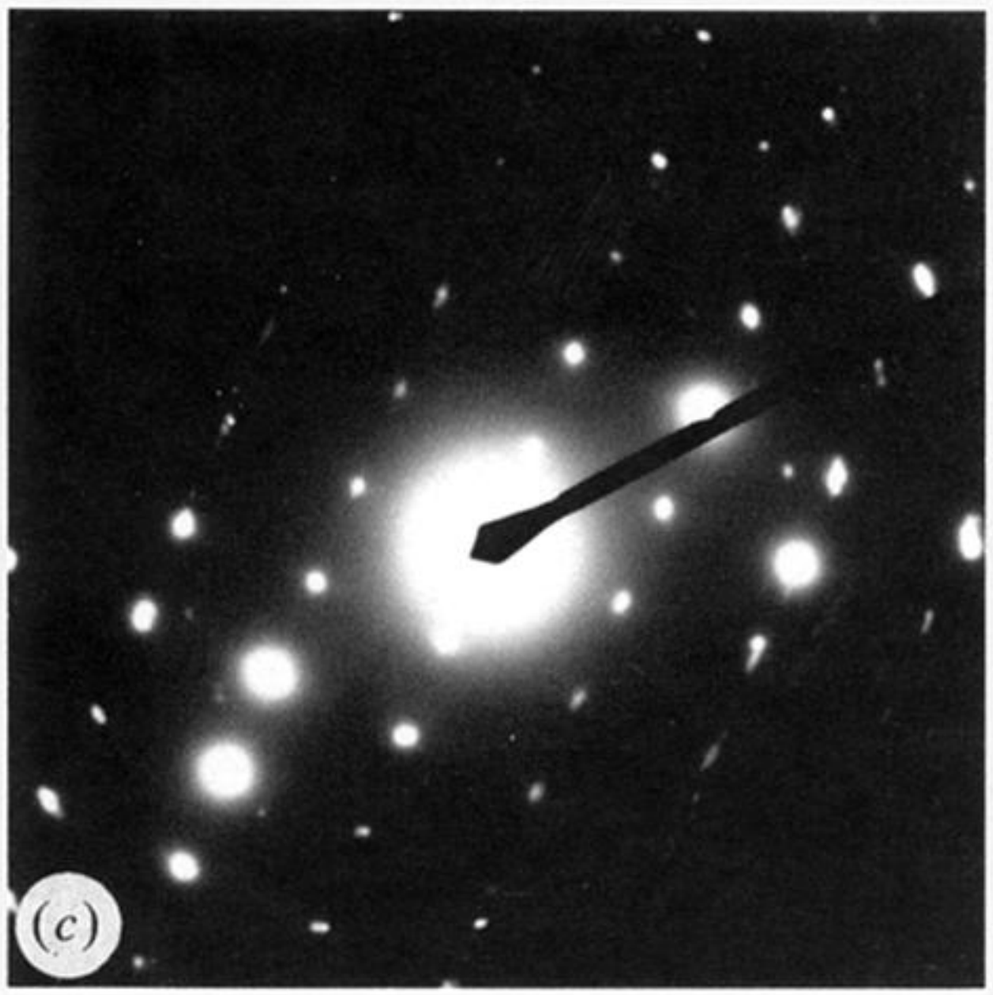

gure 14. (*a*) TEM image of the boundary zone between first order lamellae in *Littorina littorea*, indicating terlocking of the ends of the third order lamellae. Arrows point to moiré patterns formed where overlapping parts the lamellae are slightly misorientated. The SAD (inset) consists of two superposed [100] zone axis patterns.) [100] zone axis SAD obtained from lower part (A) of (*a*). (*c*) [100] zone axis SAD obtained from lower part (B) of).